MICROCOPY RESOLUTION TEST CHART
NATIONAL BUREAU OF STANDARDS-1963-A

①

AD-A186 444

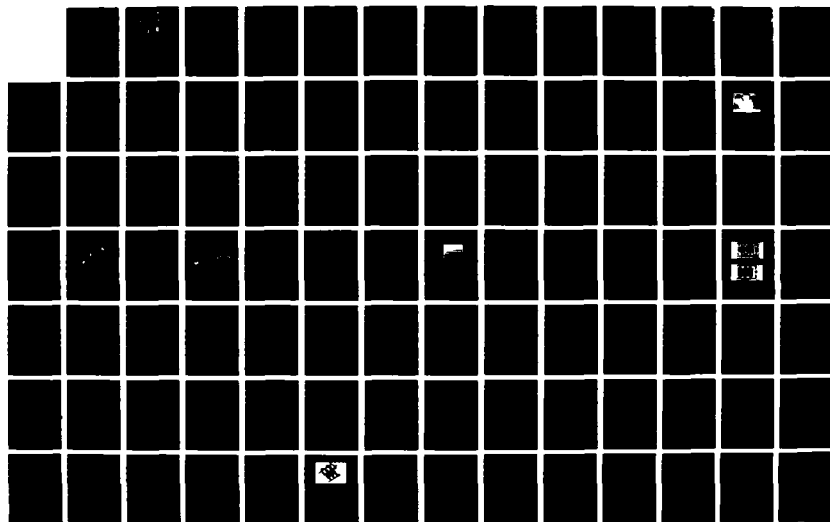# DURABILITY AND DAMAGE TOLERANCE OF ALUMINUM CASTINGS

DTIC
ELECTE
OCT 2 2 1987
S D
D

M.W.OZELTON
G.R.TURK

NORTHROP CORPORATION
AIRCRAFT DIVISION
ONE NORTHROP AVENUE
HAWTHORNE, CALIFORNIA 90250

MATERIALS LABORATORY
AIR FORCE WRIGHT AERONAUTICAL LABORATORIES
WRIGHT-PATTERSON AFB, OHIO 45433-6533

87 10 6 100

REPORT DOCUMENTATION PAGE

1a. REPORT SECURITY CLASSIFICATION	1b. RESTRICTIVE MARKINGS
UNCLASSIFIED	

2a. SECURITY CLASSIFICATION AUTHORITY	3. DISTRIBUTION/AVAILABILITY OF REPORT
2b. DECLASSIFICATION/DOWNGRADING SCHEDULE	UNLIMITED

4. PERFORMING ORGANIZATION REPORT NUMBER(S)	5. MONITORING ORGANIZATION REPORT NUMBER(S)
NOR 87-85	

6a. NAME OF PERFORMING ORGANIZATION	6b OFFICE SYMBOL (If applicable)	7a NAME OF MONITORING ORGANIZATION
Northrop Corporation Aircraft Division	3872/62	Air Force Wright Aeronautical Laboratories

6c. ADDRESS (City, State, and ZIP Code)	7b ADDRESS (City, State, and ZIP Code)
1 Northrop Avenue Hawthorne, CA 90250	AFWAL/MLSE Wright-Patterson AFB, OH 45433

8a. NAME OF FUNDING/SPONSORING ORGANIZATION Air Force Wright Aeronautical Laboratories	8b OFFICE SYMBOL (If applicable)	9 PROCUREMENT INSTRUMENT IDENTIFICATION NUMBER
		F33615-85-C-5015

8c. ADDRESS (City, State, and ZIP Code)	10. SOURCE OF FUNDING NUMBERS			
	PROGRAM ELEMENT NO	PROJECT NO	TASK NO	WORK UNIT ACCESSION NO
Wright-Patterson AFB, OH 45433				

11. TITLE (Include Security Classification)

DURABILITY AND DAMAGE TOLERANCE OF ALUMINUM CASTINGS (UNCLASSIFIED)

12. PERSONAL AUTHOR(S)
M. W. Ozelton, G. R. Turk

13a. TYPE OF REPORT	13b TIME COVERED	14 DATE OF REPORT (Year, Month, Day)	15 PAGE COUNT
Interim	FROM 9/1/85 TO 5/31/87	1987, September	108

16. SUPPLEMENTARY NOTATION

17 COSATI CODES			18 SUBJECT TERMS (Continue on reverse if necessary and identify by block number)
FIELD	GROUP	SUB-GROUP	Aluminum Castings, A357, A201, Mechanical Properties, NDI, Specifications, Regression Analyses, Composition, Heat Treatment, Solidification Rate, Microstructure

19. ABSTRACT (Continue on reverse if necessary and identify by block number)

The results from the initial 21 months of the program are presented. They include (a) an assessment of ... ... castings, and (b) the effect of process variables on the mechanical properties and microstructure of A357-T6 and A201-T7.

A new ultrasonic NDI method called Frequency Attenuation Inflection (FAI) was evaluated for determining the type and amount of defects in A357 and A201 aluminum castings. A low frequency eddy current method for detecting the presence of cracks through face sheet and fasteners was assessed.

Relationships among chemical composition, heat treatment, solidification rate, microstructure, and mechanical properties of the premium quality casting alloys A357-T6 and A201-T7 were investigated.

20 DISTRIBUTION/AVAILABILITY OF ABSTRACT	21 ABSTRACT SECURITY CLASSIFICATION
☐ UNCLASSIFIED/UNLIMITED ☒ SAME AS RPT ☐ DTIC USERS	UNCLASSIFIED
22a NAME OF RESPONSIBLE INDIVIDUAL	22b TELEPHONE (Include Area Code)	22c OFFICE SYMBOL

DD FORM 1473, 84 MAR

83 APR edition may be used until exhausted
All other editions are obsolete

ABSTRACT

The results from the initial 21 months of the program are presented. They include (a) an assessment of NDI methods for castings and (b) a determination of the effect of process variables on the mechanical properties and microstructure of A357-T6 and A201-T7.

A new ultrasonic NDI method called Frequency Attenuation Inflection (FAI) was evaluated for determining the type and amount of defects in A357 and A201 aluminum castings. Results were compared with standard X-ray radiography and microstructural investigations. The effects of surface roughness, material thickness, and nonparallel surfaces on the FAI results were determined.

An in-service low frequency eddy-current method was evaluated for detecting the presence of cracks in A201 and A357 substructures through various face sheet thicknesses using both titanium and steel fasteners.

Relationships among chemical composition, heat treatment, solidification rate, microstructure, and mechanical properties of the premium quality casting alloys A357 and A201 in the T6 and T7 conditions, respectively, were investigated. Tensile, notched tensile, and fatigue life properties, as well as microstructural features, were determined as a function of solidification rate, aging treatment, and alloy composition. Multiple regression analyses were conducted to determine correlations among the process variables and mechanical properties. Sr and Ag had the most significant effects on the properties of A357-T6 and A201-T7, respectively.

DTIC
COPY
INSPECTED
6

Accesion For

NTIS	CRA&I	☑
DTIC	TAB	☐
Unannounced		☐
Justification		

By ....

Distribution /

Availability Codes

| Dist | Avail and / or Special |

A-1

iii

Preface

CONTENTS

CONTENTS

LIST OF FIGURES

LIST OF FIGURES

LIST OF FIGURES

SECTION 1

INTRODUCTION

The use of castings for aircraft applications offers the potential for significant cost and weight savings compared with built-up structures. Recurring cost reductions greater than 30 percent are possible through reduced machining and assembly costs. Weight savings can be achieved, for example, by eliminating lap joints and fasteners. Castings allow greater shape flexibility compared with built-up structure and a reduction in the number of fastener holes, which decreases the number of potential flaw sites.

However, castings are not currently used in fatigue-critical aircraft structure because of (a) the inability to inspect thick sections and (b) a lack of durability and damage tolerance (DADT) data and design allowables that take into account the effects of inherent casting discontinuities and microstructural features on service life. The absence of the required DADT data for castings precludes compliance with the current military DADT specifications, MIL-A-83444 and MIL-A-87221. As a result, it is not possible to take advantage of the inherent cost and weight savings of castings for fatigue-critical aircraft applications.

The purpose of the "Durability and Damage Tolerance of Aluminum Castings" (DADTAC) program is to (a) investigate a nondestructive inspection technique that has the potential for providing a quantitative assessment of the discontinuities present in aluminum castings, (b) identify the process variables and discontinuities that influence the DADT properties, and (c) characterize the DADT properties of the aluminum casting alloys A357 and A201. On completion of the program, revisions to material, process, and DADT specifications will be recommended, if necessary.

This interim report covers work conducted during the first 21 months of the program under Tasks 1 and 2 of Phase I (see Section 3 for further details). NDI investigations and the effects of process variables on the properties of A357-T6 and A201-T7 castings are described.

1

SECTION 2

OBJECTIVE

The overall objective of the program is to generate durability and damage tolerance data of premium quality aluminum castings and advance foundry technology to expedite the use of these castings in primary aircraft structure. In addition, recommendations for modifying material, process, and DADT specifications will be made as required.

SECTION 3

PROGRAM APPROACH

The program consists of three phases. A brief description of the technical activity associated with each phase is provided below.

Phase I - DADT of Aluminum Castings Quality Assessment

Task 1 Up-to-date NDI methods were evaluated, using the expertise of the program NDI consultant, Dr. L. Adler of Ohio State University, to select a new NDI technique for determining the soundness of the cast plates and components tested during the program. Precise knowledge of the size, location, and types of discontinuities in the test castings was essential so that detected defects could be related to radiographic soundness.

Task 2 Concurrent with Task 1, the effects of process variables on the DADT properties of A201-T7 and A357-T6 were assessed. Screening tests were conducted to identify the process variables that provided the best balance of tensile and DADT properties for each of the two alloys. Additional castings will be made using the process variables that provide the best overall properties. The DADT properties of the optimized alloys will be comprehensively characterized and this material will become the baseline for the remainder of the program.

Task 3 The effects of discontinuities and metallurgical features (microstructure) on the DADT properties of A357-T6 will be determined using the material and process specifications developed in Task 2. For A201-T7, only the effect of microstructure will be determined.

Task 4 The applicability of the MIL-A-83444 and MIL-A-87221 specifications to A357-T6 and A201-T7 aluminum castings will be assessed, based on the data generated in Tasks 1-3.

Phase II - DADT of Aluminum Castings Quality Verification

During Phase II a DADT property validation assessment using a cast aircraft component will be performed. After considering several existing castings, one that meets the program requirements will be chosen. Four castings of the selected design will be produced based on the processing and material specification guidelines from Phase I, and will then be subjected to NDI and DADT property evaluations. The results of the testing will be compared with those obtained during Phase I to ensure that the process requirements can be scaled up from small cast plates to a large aircraft casting.

Phase III - DADTAC Program Data Consolidation

In Phase III, the results of Phases I and II will be consolidated. Material and process specifications, including any necessary silicon modification and NDI requirements, will be prepared for use in producing premium quality aluminum castings for primary aircraft structure. Necessary modifications to existing damage tolerance specifications, such as MIL-A-83444 and MIL-A-87221, will be identified and pursued as required.

SECTION 4

PHASE I, TASK 1 - NDI ASSESSMENT

4.1 INTRODUCTION

The objectives of this task were (a) to evaluate and select the most promising nondestructive inspection (NDI) method for detecting and quantifying casting defects, and (b) to evaluate an eddy current technique for detecting the presence of cracks similar to those sometimes found in aircraft component substructure.

To implement castings in fatigue critical applications, defects in cast components must be detected and quantified to assure acceptable durability. Inspection of castings for internal defects has conventionally been accomplished by X-ray radiography. However, radiography sensitivity is limited to detecting defects that are greater than about 1% of the part thickness. As part thickness increases, the minimum detectable flaw size increases and small flaws may not be detected. With these limitations, defects that may be detrimental to mechanical properties may remain undetected in thicker sections.

NDI methods were evaluated to select an alternate or complementary method to radiography that would allow both qualitative and quantitative assessment of defects in castings that are thicker than 0.75 inch. A survey of available NDI methods under development in industry and universities was conducted to select a method that showed promise. An ultrasonic technique named Frequency Attenuation Inflection (FAI) was chosen for use on the program because of the promising results shown during initial evaluations by Northrop before commencing the contract activities. Also, the equipment to perform FAI evaluations is relatively simple and inexpensive, and is easily adaptable for potential application by foundries. The FAI technique was developed by Dr. L. Adler [1] at Ohio State University (OSU) and tailored for this program through a cooperative effort between Dr. Adler and Northrop NDI personnel.

Development of the technique was accomplished through evaluations of A357 and A201 cast plates of different thicknesses that contained a range of typical casting defects. A total of 34 A201 and A357 plates in two thicknesses were cast (1.25 inch and 3.0 inch). Each plate was inspected using standard radiography with a 1% sensitivity and ultrasonic C-scan methods. Six of the 34 plates that contained representative amounts and types of casting defects were then selected, based on the radiographic and C-scan results, for a detailed NDI analysis. The detailed analysis consisted of inspecting the six plates using the FAI technique, followed by slicing the as-cast plates into thinner

7

plates and reinspecting the slices using radiography, C-scans, and the FAI method. Microstructural analyses of the defects using image analysis were also conducted to measure the amount of defect present. The results of the microstructural and NDI analyses were then compared to assess the accuracy of the FAI technique compared with the conventional methods for detecting defects in castings. The effects of surface roughness and nonparallel surfaces on the defect detection sensitivity of the FAI technique were also determined. Cast surfaces are often not flat or parallel, and the effect of these conditions on defect detection capabilities must be evaluated. In addition, welding defects were intentionally produced in two otherwise defect free plates and were evaluated by X-ray, C-scan, and FAI methods. Discontinuities in castings are usually repaired by welding, and any defects incurred from welding must be detected.

In the second portion of Task 1, an eddy current technique for detecting cracks emanating from fastener holes was evaluated. Cracks originating from fastener holes are the most common in-service flaws and can be difficult to detect without removing the fasteners. The eddy current method was developed for wrought material structures by Northrop under an Air Force contract (F33615-81-C-5100) entitled "Manufacturing Technology for Advanced Second Layer NDE System." The approach in the current program was to prepare simulated component substructures from A357 and A201 with fatigue-induced cracks of different lengths emanating from holes. Face sheets of 7075-T6 of three different thicknesses were fastened to the pre-cracked subcomponents using steel or titanium fasteners, and the eddy current technique was used to detect the presence of the cracks. The two types of fasteners were used because steel (magnetic) and titanium (nonmagnetic) require the use of different probes and separate crack detection evaluation methods. Both the location and the magnitude of the cracks were determined. The results were compared with the known location and dimensions of the fatigue-induced cracks.

4.2 NDI METHODS

4.2.1 FAI Technique

The equipment used for the FAI evaluations consisted of an ultrasonic transducer mounted on a traveling bridge assembly. Ultrasonic pulse signals were transmitted through water to the casting and were reflected back to the transducer and monitored by a computer. The time delays in signal transmission/reception and the changes in the signal characteristics were then analyzed using the computer to give the pore size and overall average percent porosity in the area under the transducer.

Figure 1 is a block diagram that illustrates the FAI system. The computer digitized and stored the ultrasonic waveforms and performed the defect parameter calculations. A transducer and pulser/receiver with usable bandwidths between 2 and 20 megahertz
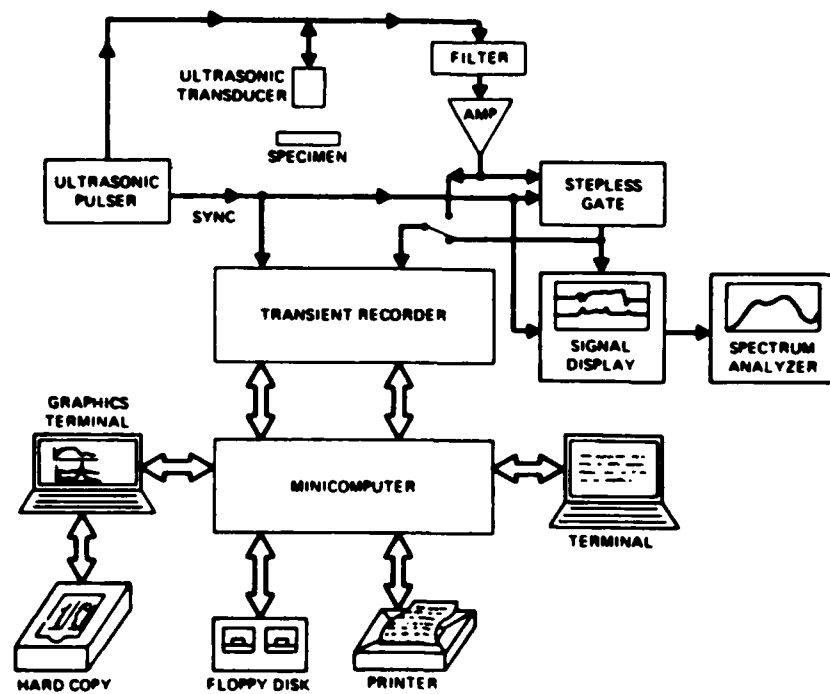
Figure 1. FAI Equipment

were used to generate ultrasonic pulses. Both the front and back surface echoes were digitized and stored using a Tektronix transient digitizer. Waveforms were digitized with a temporal resolution of less than two nanoseconds between points. Control over gating and gain was exercised by the computer. The distance from the transducer to the front surface of the plates and the specimen thickness were determined by the computer from the time delays required in gating. Waveforms were time-averaged to reduce noise. A correlation routine was used to remove the effects of electrical and mechanical jitter during waveform averaging. Using this routine, the shift in time between waveforms due to jitter was determined before the waveforms were averaged. Waveforms were then shifted by the appropriate time delay and averaged.

The frequency spectrums of the front and back surface waveforms were calculated using a fast Fourier transform algorithm. Figure 2 shows typical front and back surface echoes and their resulting frequency spectra. The spectrum of the back surface signal is deconvolved by the spectrum of the front surface signal. Attenuation coefficients, with appropriate corrections for all geometric losses, are obtained for the selected frequency range. The inflection or turning point in the attenuation versus frequency plot is used to determine the average pore size and volume fraction in the cylindrical volume sampled by the transducer. Inflection occurs at the intersection of the low frequency and high frequency scattering parameters and is dependent on pore size.

For isotropic materials, a fairly sharp peak in the derivative of the attenuation versus frequency curve is predicted by theory and observed in experiment [2]. This peak occurs for aluminum at an average pore radius R (in cm) of

$$R = 0.108/f_p \qquad \text{Eq. 4-1}$$

where f_p is the frequency in megahertz at which the peak occurs, and 0.108 is a factor accounting for the effective size of a pore and Poisson's ratio.

The average percent porosity, C, was determined by measuring the attenuation at f_p, and calculated using the following equation [2]:

$$C = 122 \cdot \alpha_p \cdot R \qquad \text{Eq. 4-2}$$

where α_p is the attenuation in nepers/cm at f_p, R is the average pore radius in cm, and 122 is a factor which is related to the average cross-section of a pore and to Poisson's ratio. The mathematical assumptions made in developing the FAI technique were based on the assumption that the defects are spherical.

The equations for R and C (Eq. 4-1 and 4-2, respectively) do not account for multiple scattering of the ultrasonic waves by
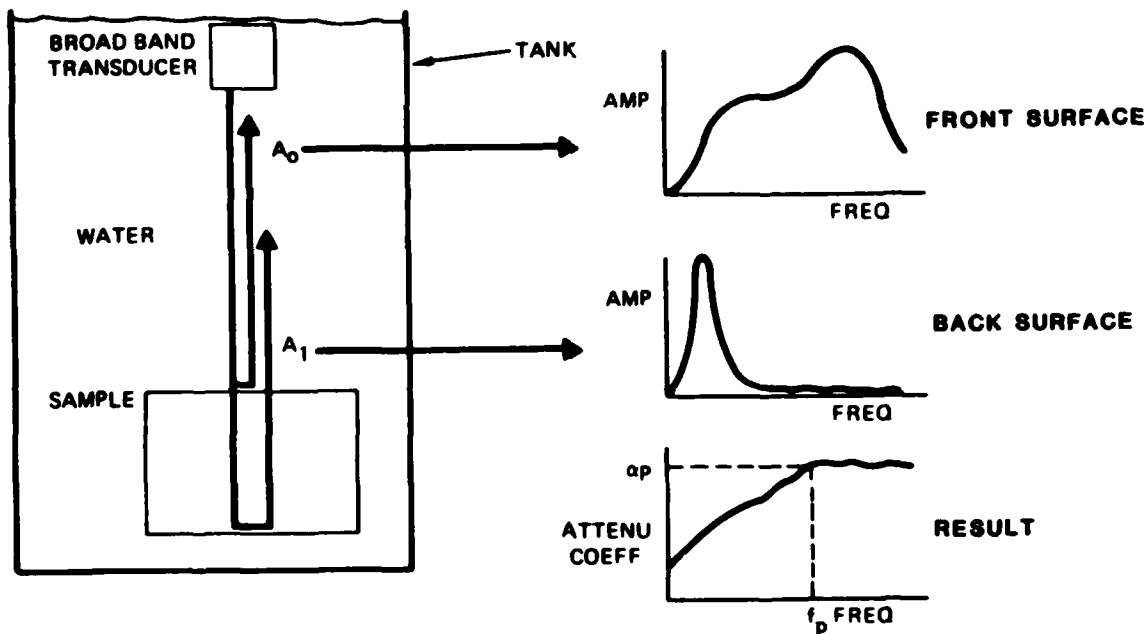
Figure 2.   Schematic Illustration of the FAI Method.

the pores, which makes the equations accurate only for relatively low levels of porosity (<6%). This is a common assumption in calculations of this type [2]. The amount of porosity found in cast materials is usually less than 6% (see Section 5.3.2), indicating that this assumption is unlikely to introduce a large error in calculating the percent porosity and pore radius.

An attenuation correction factor due to scattering of the ultrasonic waves from grain boundaries was not included in the preceding calculations due to its relatively minor effect on ultrasonic scattering compared to that caused by porosity. However, during the course of the program a lower limit for percent porosity of 0.2% was determined experimentally for the FAI technique due to grain boundary effects. Below 0.2% porosity, the ultrasonic waves scattered by grain boundaries alter the waves reflected by the pores.

4.2.2 Ultrasonic C-Scan

A block diagram of the ultrasonic C-scan system used for casting evaluations is shown in Figure 3. A DEC PDP 11/23 computer was used for data acquisition and storage, and for control of the transducer mounted on the bridge assembly. A Gould image processor was used to manipulate the data and then present them on a monitor.

A pulse/echo arrangement with a 0.5-inch-diameter, 10 MHz, center frequency ultrasonic transducer and 5.9 inch focal distance was used for the C-scans. Specimens were scanned using a point-to-point resolution of 0.04 inch. The peak magnitude of the back surface echo was digitized to 12 bits resolution. Attenuation levels of the resulting C-scans were displayed on a monitor in eight bit gray scale for analysis.

4.2.3 Radiography

Radiographs achieving a 1% sensitivity were taken of the defect-containing plates by the foundries and a Northrop-approved X-ray laboratory and were evaluated according to ASTM specification E155.

4.2.4 Eddy Current Technique

The combination of materials used for the in-service inspection investigation are shown in Figure 4, and an example of the face sheet, substructure, and eddy current probe test setup is shown in Figure 5. Three thicknesses of 7075-T6 face sheets were used in conjunction with both A357-T6 and A201-T7 substructure. A total of five different crack lengths were produced in 0.25-in.- and 0.75-in.-thick A357 and A201 fatigue specimens by constant amplitude fatigue loading. Both steel and titanium fasteners were used in the evaluations to determine their effect on the crack detection capabilities of the technique.

12
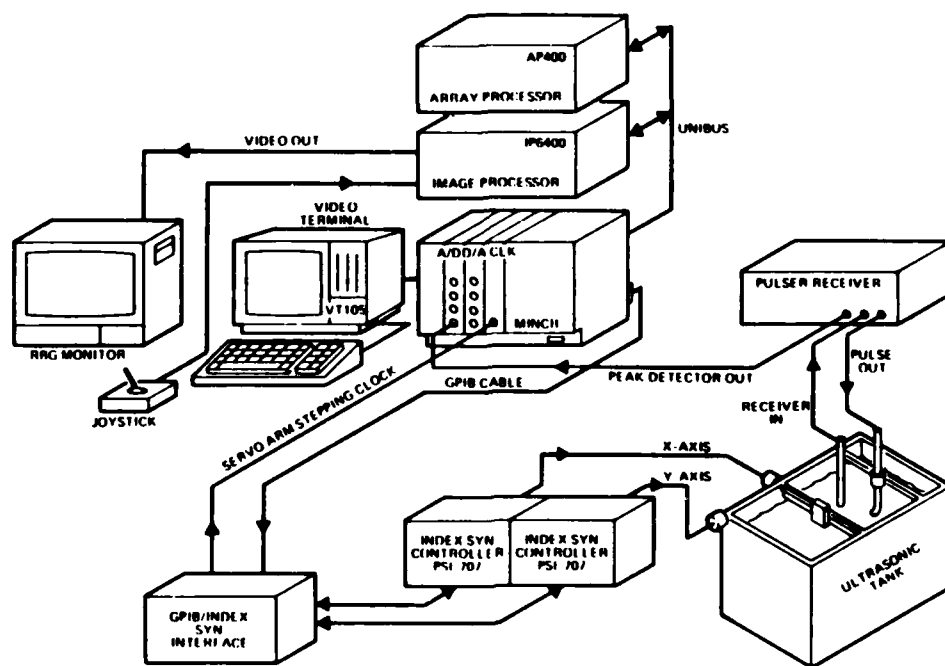
Figure 3.   C-Scan Ultrasonic Imaging System.
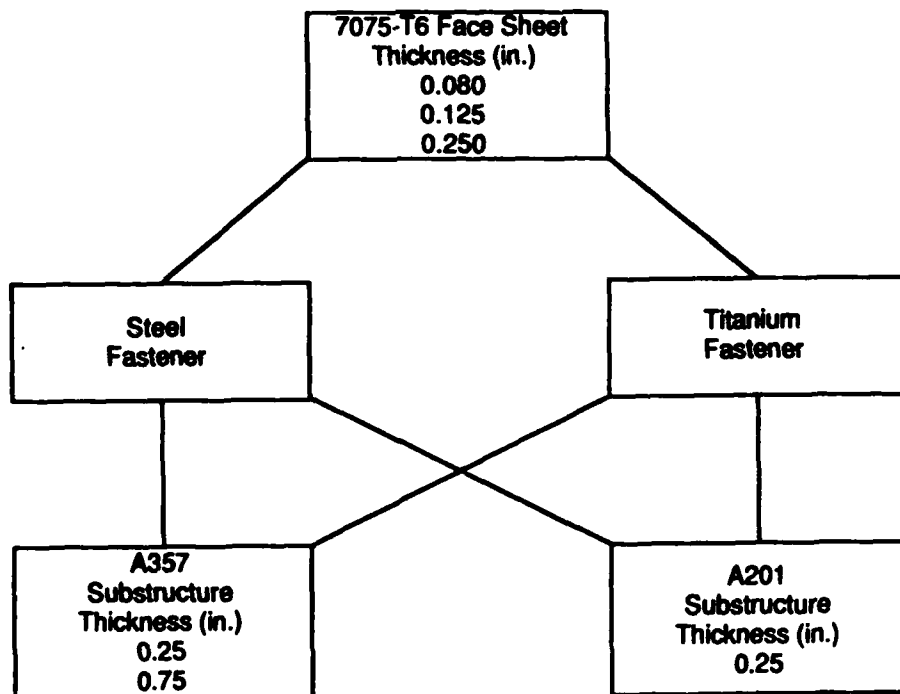
Figure 4. Combinations of Face Sheet, Fasteners, and Substructure Used for In-Service Eddy Current Inspection.
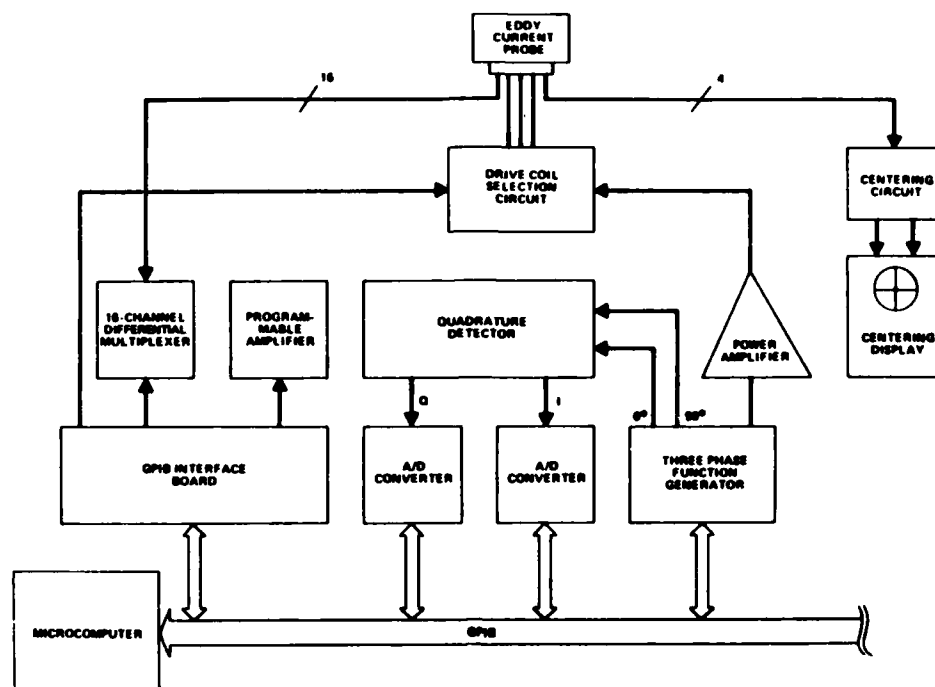
Figure 5.   In-Service Eddy Current Inspection Test Setup.

Two multisegment eddy current probes capable of detecting flaws in both the first and second layers of bolted aluminum structures were used in these investigations. A sketch depicting the differences between the two probes is shown in Figure 6, and a photograph of the probe used with the steel fastener is shown in Figure 7. The probes consist of a central drive coil and an outer ring segmented into 16 separate sensing coils. The drive coil generates an eddy current which encircles the fastener and penetrates into the face sheet and underlying substructure. Cracks in substructure fastener holes cause a perturbation of the eddy current and are detected as a change in the open circuit voltage of the sensing coils. The crack length and location can be determined simultaneously without moving the probe or removing the fastener.

A graphical representation of a low frequency eddy current probe response to substructure fastener hole cracks is shown in Figure 8. The two peaks on the graph indicate that the substructure contained two cracks located at positions number 6 and 14. The crack lengths were 0.24-in.- and 0.26-in.-long, and compared well with the optical measurements of 0.227 in. and 0.257 in. The derived crack lengths were determined from the output of the eddy current probe (in millivolts), using an empirically determined conversion factor which depends upon the thickness of the face sheet and substructure as well as the face sheet, substructure, and fastener materials. Determination of the conversion factor for different applications is conducted through an evaluation of a standard which incorporates a known crack length and the same material types and thickness as those to be inspected.

4.3   DEFECT-CONTAINING PLATES FOR FAI METHOD EVALUATIONS

Thirty-four cast plates that contained gas porosity, gas holes, shrinkage porosity, shrinkage sponge, cold shuts, and less-dense and more-dense foreign material were cast specifically for this task by ALCOA (A357) and Hitchcock Industries (A201). The alloys, defect types, and plate thicknesses are listed in Figure 9. All plates were 6-in. by 6-in. by 1.25-in.- or 3-in.- thick. Two defect-free plates were also cast for evaluation of welding defects (lack of penetration, lack of fusion, porosity, and cracks).

The gas defects were produced by intentionally not degassing the melt, pouring at a higher than normal melt temperature, adding ammonium chloride wrapped in aluminum foil to the melt, or blowing argon gas into the mold during pouring. Shrinkage defects were produced by nonoptimum chill and riser placement. The cold shut was produced by interrupting the pour. Less-dense foreign material was introduced into the casting by overagitating the melt to capture aluminum oxide in the molten aluminum, by pouring the melt into the risers instead of the pouring cup, or by removing all filters and screens from the runner system. The

16
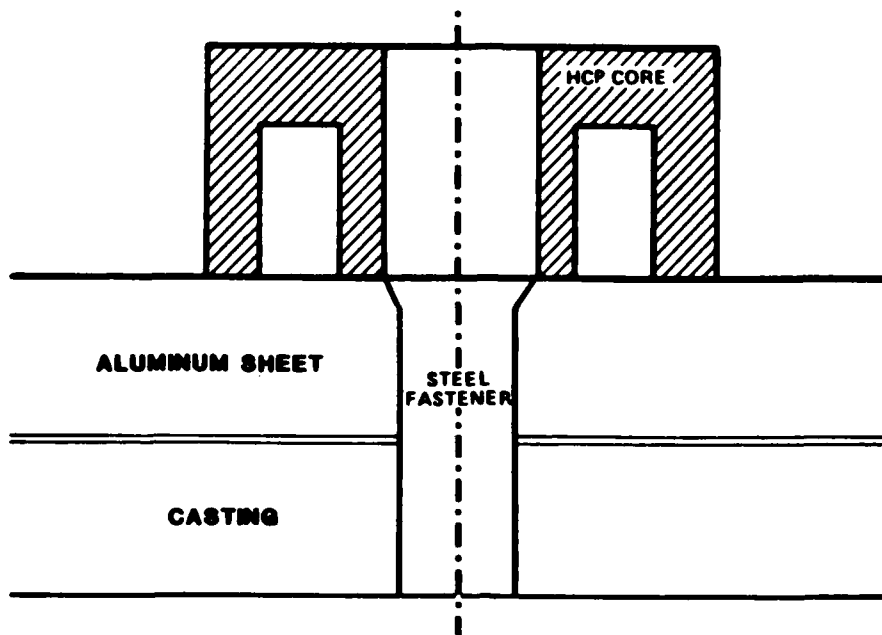
(a) Steel Fastener (Magnetic) - Hollow Center Probe (HCP)
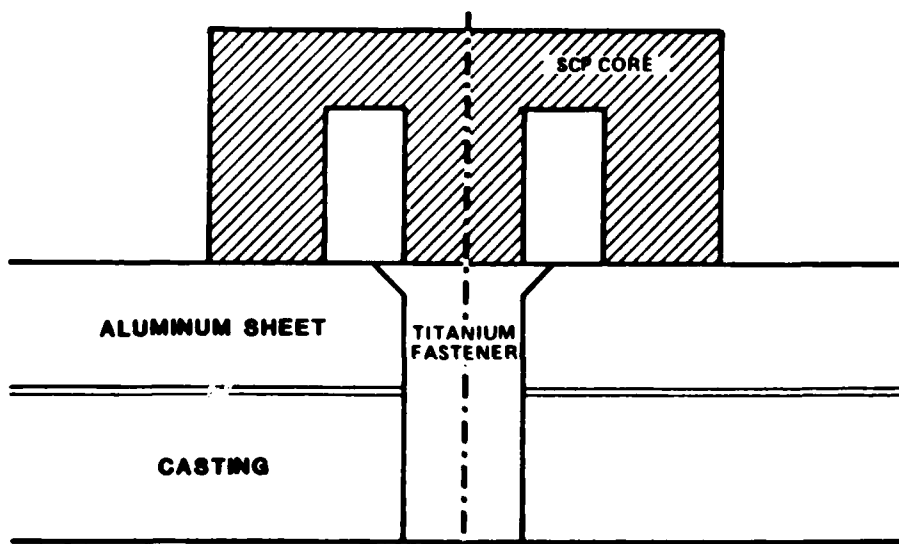
(b) Titanium Fastener (Nonmagnetic) - Solid Center Probe (SCP)

Figure 6. Schematic Illustration of the Probes Used With Steel and Titanium Fasteners.
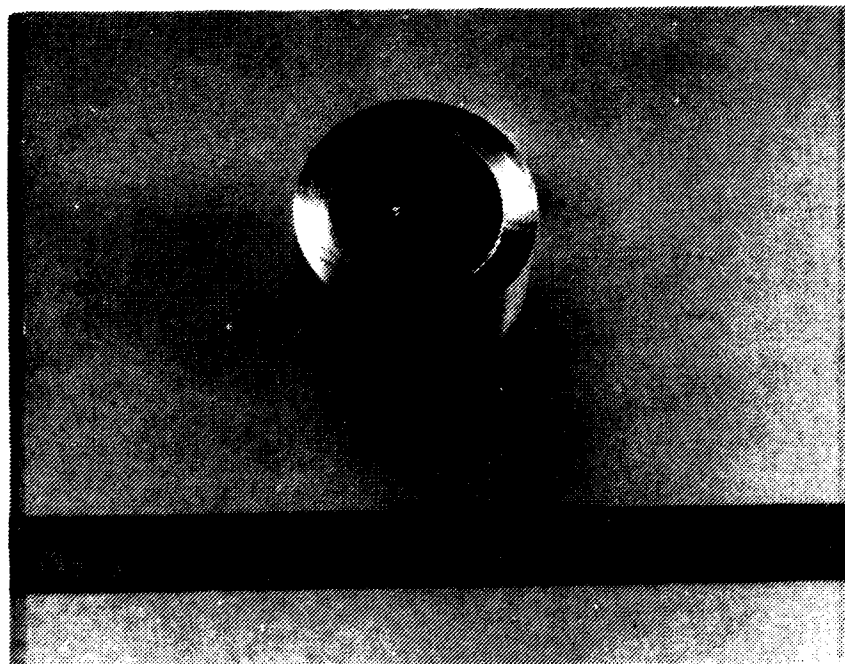
Figure 7.   Multisegment Eddy Current Probe.
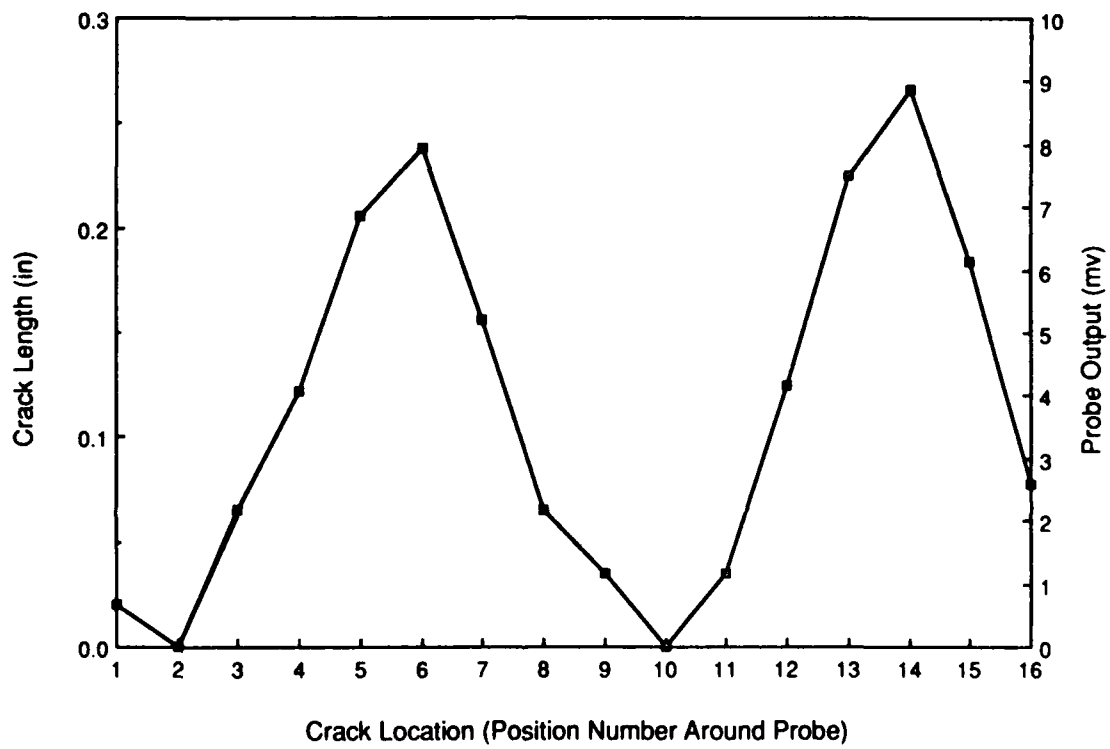
Figure 8.   Typical Eddy Current Probe Output.

| DEFECT | GRADE[1] | PLATE THICKNESS[2] (in.) | | A201 |
| | | A357 | | |
		1.25	3.0	1.25
Gas Holes	B	X	X	X
Gas Porosity	B	X	X	X
	C			
Shrinkage Cavity	B	X	X	X
	C	X	X	X
Shrinkage Sponge	B	X	X	X
	C	X	X	X
Less Dense Foreign Material	B	X	X	X
	C	X	X	X
More Dense Foreign Material	B	X	X	X
Cold Shut	B	X	X	X
Segregation	B	–	–	X
Weld Repair Defect	B	X	–	X

(1) According to MIL-A-2175.
(2) All plates were 6 in. x 6 in. x the indicated thickness.

Figure 9.   Defect Types and Plate Thickness of A357 and A201 Defect-Containing Plates.

20

more-dense foreign material defects were obtained by introducing tungsten and iron filings into the melt during pouring.

The weld defects, lack of penetration and fusion, porosity, and cracks, were produced by using non-standard GTA welding procedures. Dirty electrodes were used, the surfaces of the castings were not cleaned, plates were improperly heated, and the weld grooves were intentionally not filled.

4.4 RESULTS AND DISCUSSION

The defect-containing plates used for the FAI evaluations were initially screened using X-ray radiography and C-scans. The objective of the screening process was to identify six plates that provided a selection of alloy/defect/plate thickness combinations for detailed FAI evaluation. The six plates that were selected are described in Figure 10 and were selected because (a) the defects were well-dispersed, (b) they offered a comparison of the defect detection capability for different plate thicknesses, and (c) in most cases more than one grade (A/B, B, C) was available for a given defect. The six plates were initially evaluated by Dr. Adler at Ohio State University (OSU) and then by Northrop to determine if similar results could be obtained.

All six plates were initially evaluated with sandblasted surfaces, which represented an as-cast or finished casting surface. Both surfaces of each plate were then machined smooth and the evaluation was repeated to determine the effect of surface roughness on the FAI results. The plates were cut into slices, which were then evaluated. A comparison was made between the results for the thinner slices and those for the full-thickness plates. The slices had machined surfaces.

After completing the FAI evaluation on the slices, areas of several plates were selected for microstructural characterization to provide a comparison between the results obtained microstructurally and those predicted from the FAI analysis. In addition, FAI results for plates with nonparallel sides were obtained because many castings have complex shapes.

For the in-service eddy current inspection effort, fatigue cracks were induced from fastener holes in A357 and A201 specimens. Face sheets of three thicknesses of 7075-T6 were installed over the precracked substructure using steel or titanium fasteners. The effectiveness of the eddy current method for qualitatively and quantitatively detecting the presence of the cracks was evaluated.

The results from the evaluations outlined above are discussed in the following subsections.

21

ALLOY	THICKNESS (INCH)	DEFECT	TARGET GRADE
A201	1.25	Shrinkage Sponge	B
	1.25	Less Dense Foreign	C
A357	3.0	Gas Porosity	B
	1.25	Gas Porosity	B
	3.0	Less Dense Foreign	B
	3.0	Shrinkage Sponge	B/C

Figure 10. Defect Plates Selected for FAI Evaluation

4.4.1 FAI Evaluation of the Full-Thickness Plates

Prior to conducting the FAI tests, a grid consisting of nine 2 inch x 2 inch squares was marked on one surface of each plate and each square was identified with a number from 1 to 9. Both Dr. Adler and Northrop conducted measurements at the center of each of the nine squares using a 0.5-inch-diameter probe, so that the data from the two sources could be compared. The results are shown in Figures 11 and 12, which include the pore radius and average percent porosity data for sandblasted and machined (smooth) surfaces, respectively.

Because of the plate thicknesses, an accurate radiographic assessment of defect content and grade could not be made, particularly for the 3-inch-thick plates. The grades shown in Figures 11 and 12 were those that were targeted for each plate.

The results of the joint evaluations by Northrop and Dr. Adler show that the pore radius and percent porosity data were within experimental scatter for both sandblasted and machined surfaces. Therefore, it was concluded that the FAI technology developed at OSU by Dr. Adler had been duplicated in Northrop's NDI Research Laboratory.

The differences in the average pore radius and percent porosity results for the sandblasted and machined surfaces were small. The overall trend indicated a slightly lower value for the machined surfaces than for those that were sandblasted, which is in good agreement with analytical predictions derived at OSU [3].

The average RMS roughness values for the sandblasted and machined plate surfaces were 210 and 62 microinches, respectively. The increased roughness of the sandblasted surfaces provided a higher value for pore radius and percent porosity because of increased ultrasonic wave scattering compared with the machined surface. However, a compensation factor could be developed to minimize the discrepancy. This can be accomplished by assuming a Gaussian distribution of the RMS surface roughness, which can be determined by mechanical or ultrasonic means. By fitting the spectral attenuation of the front surface echo to an analytical equation, the attenuation of the back surface echo can be calculated. A complete derivation and explanation of the effects of surface roughness on ultrasonic attenuation can be found in Reference 3.

The FAI evaluations of the plates that contained less-dense foreign material did not indicate increased ultrasonic scattering due to the presence of foreign material. The data represent low background levels of other discontinuities, such as porosity. There was no difference between these measurements and those obtained for squares in the same plate that did not contain foreign material. Thus, it was concluded that the FAI method cannot be used for detecting the presence of less-dense foreign

23

DEFECT/ ALLOY	GRADE/ THICKNESS	AVERAGE PORE RADIUS* (μm)			
		NORTHROP		OHIO STATE UNIVERSITY	
		SAND-BLASTED	MACHINED	SAND-BLASTED	MACHINED
SHRINKAGE SPONGE/ A357	GRADE B/ 3 INCHES	79	79	77	65
SHRINKAGE SPONGE/ A201	GRADE B/ 1.25 INCH	151	139	140	119
GAS POROSITY/ A357	GRADE C/ 3 INCHES	163	151	147	133
GAS POROSITY/ A357	GRADE B/ 1.25 INCH	134	130	116	101
LESS-DENSE FOREIGN MATERIAL/ A201	GRADE C/ 1.25 INCH	67	67	61	52
LESS-DENSE FOREIGN MATERIAL/ A357	GRADE B/ 3 INCHES	60	70	**	**

*Average of nine areas per plate.
**None detected.

Figure 11. FAI Pore Radius Data for Defect-Containing Plates

DEFECT/ ALLOY	GRADE/ THICKNESS	AVERAGE POROSITY* (%)			
		NORTHROP		OHIO STATE UNIVERSITY	
		SAND-BLASTED	MACHINED	SAND-BLASTED	MACHINED
SHRINKAGE SPONGE/ A357	GRADE B/ 3 INCHES	0.3	0.3	0.3	0.3
SHRINKAGE SPONGE/ A201	GRADE B/ 1.25 INCH	1.4	1.5	1.6	1.3
GAS POROSITY/ A357	GRADE C/ 3 INCHES	0.7	0.6	0.7	0.6
GAS POROSITY/ A357	GRADE B/ 1.25 INCH	1.3	1.3	1.1	1.1
LESS-DENSE FOREIGN MATERIAL/ A201	GRADE C/ 1.25 INCH	0.4	0.2	0.4	0.4
LESS-DENSE FOREIGN MATERIAL/ A357	GRADE B/ 3 INCHES	0.2	0.1	**	**

*Average of nine areas per plate.
**None detected.

Figure 12. FAI Percent Porosity Data for Defect-Containing Plates.

material without further development. An extended feasibility study (such as that in Reference 1) is necessary to establish the detectability of different foreign materials depending on size and concentration.

4.4.2 Correlation Between FAI Results for Plates and Slices

After evaluating the six 1.25-inch- and the 3.0-inch-thick plates, they were cut into slices, each of which was about 0.6-inch-thick. Two slices were obtained from the 1.25-inch-thick plates and four or five were obtained from the 3.0-inch-thick plates. All slices were 6 inches x 6 inches in area. The surfaces of the slices were machined parallel and were marked with the same 2 inch x 2 inch square grid pattern that was used for the plates so that the NDI evaluations of the slices coincided exactly with those for the whole plates. Therefore, it was possible to provide a defect map of the thick plates from the data for the slices, which allowed a correlation of the effect of thickness on the FAI results to be made. Some material was lost due to saw cuts and machining, which represented about 15% of the original plate thickness.

Each slice was individually X-rayed by an independent laboratory that serves the casting community to determine if the soundness and the defect content were as expected and in agreement with the data obtained for the thicker plates. X-ray radiography is subject to defect detection limitations for 1.25-inch-thick material, even using a 1% sensitivity, and would detect only the very largest defects in 3-inch-thick material.

The FAI data for the plates and the slices are summarized in Figure 13, and are the average percent porosity and pore radius values for the nine squares in each plate and corresponding slices. The results for the three types of defects shown in Figure 13 are discussed separately below.

Gas Porosity Plates

X-ray radiography of the slices cut from each of the two gas porosity plates (3-inch- and 1.25-inch-thick) showed that the overall plate soundness grades were similar to those of the slices. Fifty-four individual 2 inch x 2 inch squares were graded. Of these, 36 squares were Grade B gas porosity; the remaining 18 squares were Grade C gas porosity. Twelve of the Grade C squares were in the 3-inch-thick plate.

There was a significant difference between the FAI results for the 3-inch-thick plate and corresponding slices. The average percent porosity and pore radius for the plate and slices was 0.6% and 1.4%, and 150 μm and 93 μm, respectively. For the 1.25-inch-thick plate, the differential between the plate and slice data was much less, i.e. 1.3% vs. 1.6%, respectively, for the percent porosity and 129 μm vs. 105 μm for pore radius, respectively. These differences probably result from the

26

DEFECT GRADE/ALLOY	PLATE THICKNESS (INCH)	PERCENT POROSITY		PORE RADIUS (μm)	
		PLATE[1]	SLICES[2]	PLATE[1]	SLICES[2]
Gas Porosity					
Grade B/A357	3	0.6	1.4	150	93
	1.25	1.3	1.6	129	105
Shrinkage Sponge					
Grade B/A357[3]	3	0.3	0.3	79	73
Grade B/A201	1.25	1.3	2.3	138	94
Foreign Material					
Grade B/A357	3	0.1	0.1	70	10
Grade C/A201	1.25	0.2	0.2	67	38

(1) Machined surfaces - Northrop data.
(2) All the slices were approximately 0.6-inch-thick.
(3) Plate supposed to contain shrinkage sponge, but actually contains gas porosity.

Figure 13. Correlation Between FAI Data for the Plates and Slices.

nonuniform distribution of defects and/or the dynamic range of the system, as discussed below.

Porosity assessment by FAI is based on assuming an even porosity distribution, i.e., the pore radius and the percent porosity should be the same at different depths. Since this is often not the case, the overall parameters represent an average, which is calculated from the overall ultrasonic attenuation. Therefore, the mutual effect of the percent porosity and pore radius on each other should be taken into consideration. For example, for a given pore radius, a higher percent porosity should be weighted more in the overall average pore radius than a lower percent porosity because the contribution to the total attenuation is higher. Similarly, for a given percent porosity, the contribution of smaller pores should be weighted more in the overall average percent porosity. For the data shown in Figure 13 this mutual interaction was neglected and both volume fractions and pore radii were averaged independently of the other parameter. The averages of the thin slices were compared to the overall values for the original thick plates to determine the effect of thickness on the FAI results.

The dynamic range of the system influences the ability to accurately determine the percent porosity and pore radius. Whenever the attenuation exceeds the dynamic range of the system, the resulting measured attenuation value is saturated, and the actual attenuation is underestimated. This occurs mainly in thick samples, and can be recognized easily from the detected signal. Attenuation saturation plays an important role in the FAI method by setting the limit for accurate measurement and indicating the need to increase the dynamic range of the system by spatial averaging, increasing the resolution of the system, or refinement of data reduction methods.

The dynamic range of the equipment used in the current work was 60 dB. The data for all the plates and slices were reanalyzed, taking the dynamic range into consideration (Figure 14). For the total data base (54 squares) only 57% and 52% of the pore radius and the percent porosity values, respectively, of the plates were essentially the same as those for the slices. For those areas for which the attenuation was below the dynamic range of the equipment (<60 dB), the agreement between plate and slice data improved significantly, i.e., to 91% and 85% for the pore radius and the percent porosity, respectively. Clearly, by increasing the dynamic range of the system, the discrepancies between the data for the thick plates and the slices can be significantly reduced.

Shrinkage Sponge Plates

The shrinkage sponge defect intended to be included in the 3-inch-thick A357 plate was not substantiated by an evaluation of the slices, which indicated that the plate contained mainly gas porosity. Radiography of the 3-inch-thick plate was inconclusive regarding identification of defect type and level. Five slices

POROSITY	DIFFERENTIAL BETWEEN PLATES[1] AND SLICES [2]	AGREEMENT BETWEEN PLATE AND SLICE RESULTS(%)	
		TOTAL DATA BASE[1]	DATA WITHIN 60 dB DYNAMIC RANGE[3]
Radius	< 10 μm	57	91
	10-20 μm	13	9
	> 20 μm	30	0
Percent	< 0.1%	52	85
	0.1-0.2%	9	15
	> 0.2%	39	0

(1) Nine squares from each of the 6 plates (54 squares total).
(2) Average for the squares from the slices that comprised each of the 54 squares in the plate.
(3) Only those squares for which saturation was not indicated (31 squares).

Figure 14. Effect of Dynamic Range on FAI Measurements

were obtained from this plate, providing 45 squares for FAI evaluation. The top 4 slices were graded by X-ray radiography as Grade B gas porosity. Some Grade B, C, and D foreign material was found in the bottom slice.

The 1.25-inch-thick A201 plate showed a much stronger correlation between X-ray data for the plate and the two slices. The presence of shrinkage sponge was confirmed in both slices; one slice was entirely Grade B and the other was entirely Grade D. These radiographic assessments demonstrate that certain size defects in very thick plates (3 inches) may not be detected using conventional X-ray radiography.

The average percent porosity determined by FAI for the 3-inch-thick plate that was supposed to contain shrinkage sponge and the individual slices was the same (0.3%, Figure 13). The average pore radius values were also very similar, 79 m and 73 m for the plate and slices, respectively. These data represent gas porosity and not shrinkage sponge, which was not present in the plate or slices. The results for the four slices that contained the Grade B gas porosity were significantly different from those described in the previous section, indicating that the overall correlation between FAI data and the radiographic grade is inconsistent.

For the 1.25-inch-thick A201 plate that was verified as containing shrinkage sponge, the percent porosity was 1.3% and 2.3% in the plate and slices, respectively. The corresponding average pore radii were 138 m and 94 m. The differences between the plate and slice results are consistent with those for the gas porosity data described in the previous section, and are probably also due to the defect size distribution and the limited dynamic range of the FAI system.

Foreign Material Plates

The 3-inch-thick A357 plate was Grade B according to X-ray radiography. Two of the nine squares contained less-dense foreign material (LDFM); the remaining squares contained some Grade B gas porosity. The four slices cut from the plate showed that most of the squares were Grade A/B (no observed defects). All the LDFM was in the slice cut from the bottom of the plate. Six squares were rated as Grade C for LDFM; the remaining three were Grade B gas porosity.

The 1.25-inch-thick A201 plate was rated as Grade C because of the level of LDFM in two of the nine squares. The remaining areas were Grade B gas porosity. However, of the 18 squares in the two slices cut from this plate, 17 were rated as Grade A, and one was found to contain Grade C LDFM.

The square that contained LDFM showed average pore radius and percent porosity values that were similar to the slices that were defect-free, indicating that FAI was unable to detect the

LDFM. This is discussed in more detail in the next section where the overall correlation of FAI and X-ray radiography is described.

4.4.3 Correlation Between FAI and X-Ray Assessments

All of the individual squares from the slices cut from the six defect-containing plates were individually inspected using X-ray radiography and the FAI method. All the results are shown in Figure 15. They are listed according to the various defect types and the corresponding FAI average values and ranges for percent porosity. As determined by radiography of the slices, forty-four defect-free (Grade A/B) squares were found among the total of 171 that were characterized.

The Grade A/B material had average percent porosity and pore radius values of 0.2% and 16 μm, respectively. The material that contained gas porosity and shrinkage sponge had percent porosity and average pore radius values that were significantly higher than that rated as Grade A. Statistical analysis showed that the uncertainties in the FAI values due to experimental error are about 20 μm and 0.2% for pore radius and percent porosity, respectively. Considering this experimental error margin, the specimens graded as defect-free by radiography were also found to be defect-free by FAI.

For gas porosity, the average percent porosity and pore radius values were qualitatively consistent with the X-ray radiography grades, with Grade C having higher values than Grade B. Additional data will be developed in Task 3 (Phase I) of this program, which will be statistically analyzed to try to provide pore radius and percent porosity limits that may help to differentiate quantitatively between Grades B and C. Similar trends were observed in the data for the Grade B and D shrinkage sponge (SS) material. The average measured percent porosity for Grade D SS material was slightly higher than Grade B SS material, 2.6% vs 2.1%.

The previously mentioned dynamic range limitation caused some underestimation in Grade B material, and even more in Grade C material, thereby resulting in additional overlap of FAI data for these categories.

No correlations between radiographic grade and FAI data for the LDFM defects were obtained. The percent porosity values of 0.2% were equal to those obtained for the defect free Grade A/B material. The average pore radius data also did not seem to indicate the presence of LDFM; values were similar to those obtained for gas and shrinkage porosity.

In summary, there is a qualitative correlation between FAI and X-ray radiography results for gas porosity and shrinkage sponge. The generation of additional data in Task 3 will strengthen the data base and possibly enable quantitative

GRADE	FAI DATA				
	PERCENT POROSITY		PORE RADIUS (μm)		NO. OF SQUARES EXAMINED
	AVERAGE	RANGE	AVERAGE	RANGE	
A/B	0.2	0-0.5	16	0-60	44
Gas Porosity					
B	0.7	0-2.0	70	0-140	71
C	1.6	1.0-1.9	104	70-130	22
Shrinkage Sponge					
B	2.1	1.8-2.4	93	80-110	9
D	2.6	1.4-2.9	97	80-110	9
Less-Dense Foreign Material					
B	0.2	0-0.4	78	0-110	5
C	0.2	0-0.5	54	0-110	9
D	0.2	0.1-0.3	105	100-110	2

Figure 15. Correlation Between FAI Results and X-Ray Radiographic Grade for the Plate Slices.

guidelines for differentiating between Grades B and C gas porosity and shrinkage sponge to be developed. Further development of the FAI method is required before this approach can be applied to foreign material.

4.4.4 Correlation Between FAI and Microstructural Measurements

After completing the FAI investigation of the plate slices, portions of several plates were selected for microstructural examination. The objective was to correlate the FAI-predicted data with actual microstructural measurements.

The ultrasonic probe was circular in cross section and characterized a cylinder of about 0.5-inch-diameter. The microstructural specimens were taken from the center of this circular area on the plane that was parallel with the axis of the cylinder. Image analysis was used to determine the average size of a given defect.

The selected defects and grade levels are shown in Figure 16. Typical micrographs of three types of defect (gas porosity, shrinkage sponge, and foreign material) are shown in Figures 17, 18, and 19. The average percent porosity measured using the FAI and microstructural methods for Grade B gas porosity material was 0.7% and 0.5%, respectively. For Grade C gas porosity material, the equivalent results were 1.7% and 1.3%. The agreement between FAI and microstructural data for Grades B and C was excellent. In each case, the FAI method predicted a slightly higher value than that determined from the microstructure. The overestimation of percent porosity by the FAI method is probably due to the difference in measurement methods between FAI and image analysis. The FAI values for percent porosity and pore radius are determined on a volumetric basis, while the same values obtained from microstructural analysis were determined on a cross-sectional basis. The microstructural data, therefore, do not allow a full defect evaluation because the entire defect is not sampled. In addition, the FAI values are not completely accurate due to the nonspherical shapes of the pores. The theory upon which FAI is based assumes that the pores are spherical, which is not the case in practice (Figure 17); most of the pores tend to be elliptical.

Similar to the percent porosity, the FAI average pore radius data for gas porosity were higher than those obtained by microstructural analysis. The average FAI and microstructural pore radii for Grade B porosity were 103 μm and 40 μm, respectively. For Grade C, the equivalent results were 120 μm and 91 μm. Similar to the percent porosity assessment, the measured average pore radii for Grade C material were higher than that of Grade B material. The average pore radius measurements from the FAI method were observed to be approximately equal to the longer axis of the elliptically shaped pores, which supports the conclusion that the discrepancy is related to the nonspherical nature of the gas pores.

33

DEFECT TYPE[1]/ GRADE[2]	PERCENT POROSITY		PORE RADIUS (μm)	
	FAI[3]	MICROSTRUCTURE[4]	FAI[3]	MICROSTRUCTURE[4]
GP/B	1.6	1.4	110	98
GP/B	0.1	0.05	100	12
GP/B	0.4	0.1	100	11
GP/C	1.6	1.0	110	89
GP/C	1.8	1.6	120	97
GP/C	1.6	1.4	130	86
SS/B	1.9	1.3	80	15
SS/D	2.3	1.2	80	19
LDFM/D	1.0	(5)	180	(5)

(1) GP=gas porosity; SS=shrinkage sponge; LDFM=less-dense foreign material
(2) According to MIL-A-2157
(3) Volumetric data
(4) Surface cross-section data
(5) Complex shape - specific numbers could not be assigned

Figure 16. Comparison of FAI and Microstructural Analysis Data
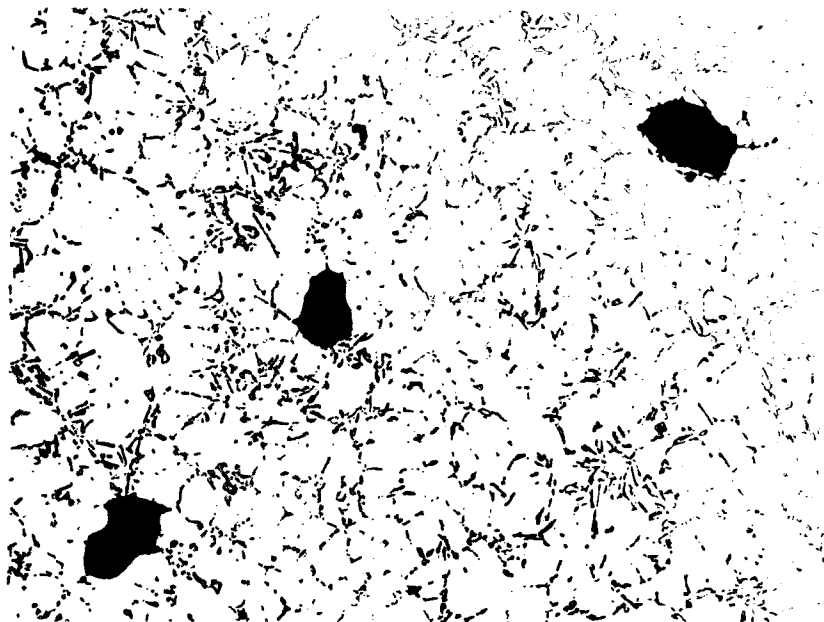
50X

Figure 17. Typical Gas Porosity in Grade C A357.

50X

FIGURE 18.   Typical Shrinkage Sponge in Grade D A201
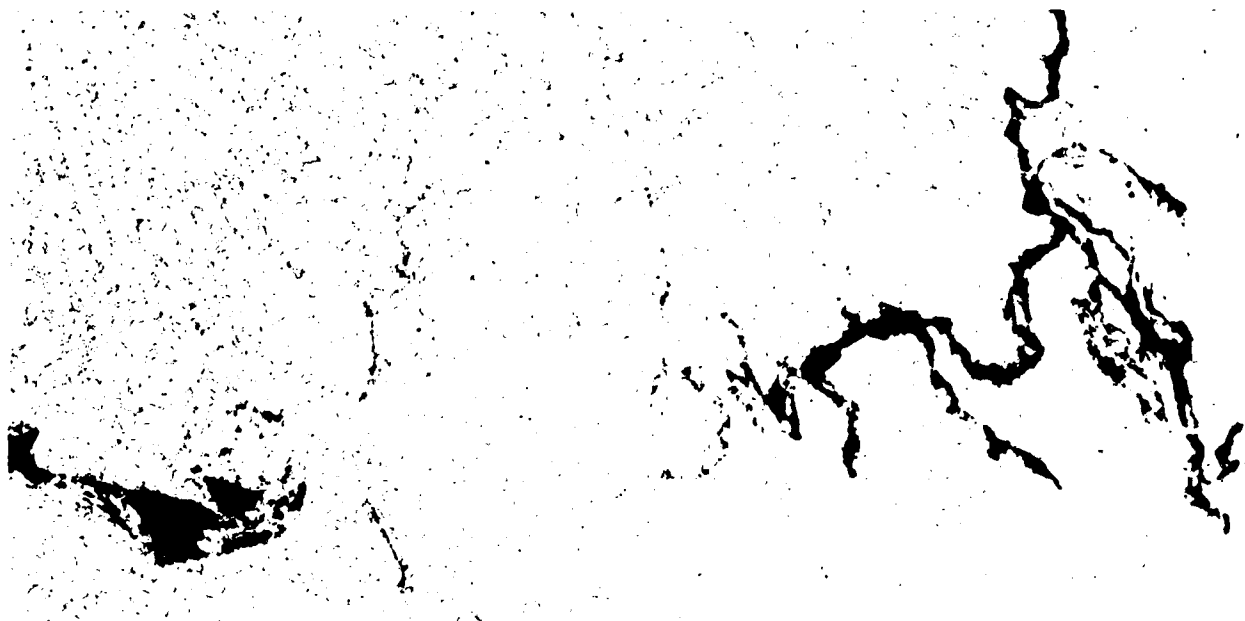
50X

Figure 19. Typical Less-Dense Foreign Material in Grade C A357

The correlation between data from the FAI and the microstructural methods for the shrinkage sponge was not as good as that for gas porosity. Two grade levels (B and D) were evaluated. The percent porosity obtained using the FAI and microstructural methods was 1.9% and 1.3%, respectively, for Grade B, and 2.3% and 1.2% for Grade D. The equivalent data for the average pore radius were 80 μm and 15 μm (Grade B) and 80 μm and 19 μm (Grade D). The FAI percent porosity data correlated better with the X-ray grades than did the microstructural results. It is difficult to attempt a correlation of this type, particularly for pore radius measurements, because of (a) the difficulty of accurately assigning a dimension to a defect that has a relatively complex shape (Figure 18), and (b) because the FAI model assumes that the defects are spherical.

The situation for foreign material was complicated. A typical LDFM inclusion has a very complex shape (Figure 19) and cannot be readily assigned specific dimensions. The deviation from a spheroidal shape is even greater than that for gas porosity and shrinkage sponge. For LDFM shown in Figure 19, the percent porosity and pore radius measurements obtained using the FAI method were 1.0% and 180 μm, respectively. The percent porosity value falls in the range typical of those for gas porosity and shrinkage sponge (Figure 16). The average pore radius (180 μm) was larger than those typical of gas porosity and shrinkage sponge. However, the LDFM (Figure 19) was much bigger than the other two defects shown in Figures 17 and 18. The data indicate that the FAI method, as currently designed, cannot accurately identify foreign materials in castings.

4.4.5 Effect of Nonparallel Surfaces on FAI Results

Because the surfaces of castings are often not parallel, the effect of nonparallel surfaces on the FAI results was determined. The measurements were performed on one of the slices discussed in Section 4.4.2. The slice was A357 and was determined by X-ray radiography and FAI measurements to have a very uniform distribution of Grade B gas porosity. Surfaces of the nine squares were machined so that they were at angles in the range of 2° to 10° compared with the opposing surface. The FAI results as a function of angle are shown in Figure 20. For a given location, the FAI measurements were taken both before (parallel sides) and after machining (nonparallel sides). The average pore radius for parallel and nonparallel sides was, within experimental scatter, the same for a given angle. However, the measured average percent porosity showed an increase from about 1.4% for parallel sides to 2.1% for the 10° angle.

The above results suggest that the effectiveness of the FAI method without further development may be reduced if the angle between opposing sides of the casting is greater than about 7° (Figure 20).

	AVERAGE PORE RADIUS[1] (μm)		AVERAGE PERCENT POROSITY[1]	
ANGLE[2]	NONPARALLEL	PARALLEL[3]	NONPARALLEL	PARALLEL[3]
0	-	100	-	1.4
2	90	100	1.6	1.5
5	100	80	1.7	1.5
7	130	110	1.9	1.6
10	110	100	2.1	1.5

(1) Data obtained for a 0.75-inch-thick slice of an A357-T6 plate that contained Grade B gas porosity.
(2) Between opposing surfaces
(3) Value before machining the angle.

Figure 20.   Effect of Nonparallel Surfaces on Defect Detection Capabilities of the FAI Technique.

4.4.6 Weld Defect Evaluation

The welding defects, i.e., lack of fusion and penetration, cracks, and porosity, were produced in one plate of both A357 and A201 using GTA welding. The defects were initially detected by both radiography and C-scan and then by the FAI method. Figure 21 shows a C-scan of the weld defects in the A357 plate. Six locations evenly spaced along each of the welds were chosen for evaluation by FAI yielding a total of 29 test locations. The defects at each of these locations were then characterized by radiography for comparison with the FAI results. None of the welds were defect-free Grade 1. All welds contained defects of Grade 2, indicating that the welds were not acceptable. Welding specifications do not assign defect Grades B, C, and D to defective welds. Instead, the welds are graded as passed (Grade 1) or failed (Grade 2).

The results of the FAI evaluations and the defect type are listed in Figure 22. Percent porosity and pore radius values were obtained at all 29 locations examined. The severity level of the defects is not determined by radiography standards, and the accuracy of the FAI results could not be exactly assessed. However, because weld defects are radiographically graded in a pass/fail manner, it was assumed that any reading greater than that obtained from essentially defect-free material indicates a defective weld. Further development of the FAI technique is required, though, to fully define the FAI values corresponding to defect-free material. Once this has been accomplished, assessment of weld quality by FAI on a pass/fail basis should be feasible.

4.4.7 In-Service Crack Detection Results

The results of the in-service inspections are summarized in Figure 23. The actual crack lengths, determined from optical measurements, are listed, along with the corresponding probe outputs and predicted crack lengths determined for each face sheet thickness/cast material/fastener combination. With the steel fastener installed, all of the cracks in both A357 and A201 were detected through each of the three face sheet thicknesses. With the titanium fastener installed, all cracks could be detected and quantified except for the shortest crack/thickest face sheet combination of 0.049 inch/0.25 inch. Difficulty in detecting this crack was due to interference between the low probe output (0.2 mv) and the system noise. The 0.049-inch-long crack could be detected and quantified through the other two face sheets, which were 0.08-inch- and 0.125-inch-thick. Based on these results, a lower threshold of about 1.0 mv should be used to account for system noise.

These results clearly indicate that this eddy current technique may be used for in-service inspections to accurately detect and measure cracks originating from fastener holes underneath face sheet materials.
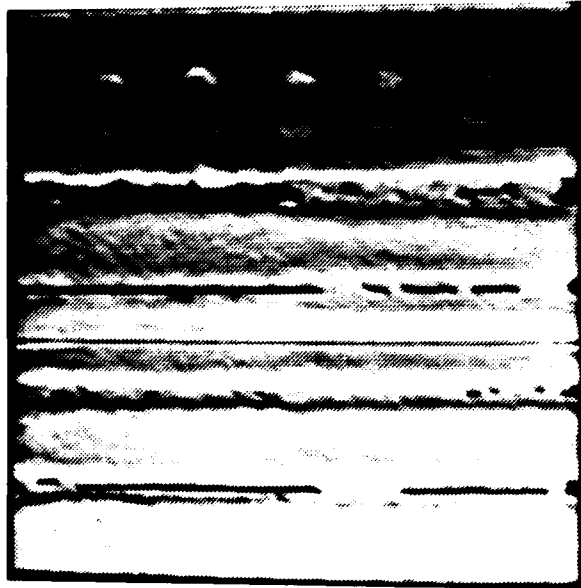
Figure 21.   C-Scan of Weld Defects in A357
             (Defects: Cracking, Lack of Penetration
             and Fusion, Porosity)

DEFECT TYPE	ALLOY	PERCENT POROSITY	PORE RADIUS (μm)
None	A357	0.4	152
	A201	0.3	65
Foreign Material	A357	0.5	91
	A201	1.2	133
Gas Hole	A357	0.3	180
Crack	A357	0.4	50
	A201	0.4	176
No Fusion	A357	0.4	150
	A201	0.4	176

Figure 22.   Results of FAI Evaluation of Plates Containing Weld Defects.

| FASTENER MATERIAL | SUBSTRUCTURE MATERIAL-THICKNESS (IN.) | ACTUAL CRACK LENGTH | 7075-T6 FACE SHEET THICKNESS (IN.) | | | | | |
| | | | 0.250 | | 0.125 | | 0.080 | |
			PREDICTED CRACK LENGTH (IN.)	PROBE OUTPUT (mv)	PREDICTED CRACK LENGTH (IN.)	PROBE OUTPUT (mv)	PREDICTED CRACK LENGTH (IN.)	PROBE OUTPUT (mv)
Steel	A357-0.25	0.049	0.05	1.0	0.04	1.6	0.04	2.1
	A357-0.25	0.141	0.15	5.0	0.14	11.0	0.14	18.7
	A357-0.75	0.257 and 0.227	0.26 and 0.24	8.3 and 7.5	0.26 and 0.23	23.9 and 20.8	0.26 and 0.25	38.8 and 37.9
	A201-0.25	0.049	0.05	1.0	0.05	2.3	0.05	3.5
	A201-0.25	0.077	0.07	1.7	0.07	3.0	0.07	6.1
Titanium	A357-0.25	0.049	0	0.2	0.05	0.9	0.06	2.9
	A357-0.25	0.141	0.14	1.8	0.14	10.3	0.13	27.3
	A357-0.75	0.257 and 0.227	0.24 and 0.24	3.7 and 3.2	0.24 and 0.23	22.0 and 19.5	0.24 and 0.24	59.8 and 59.5
	A201-0.25	0.049	0	0.4	0.05	1.3	0.06	3.7
	A201-0.25	0.077	0.07	0.9	0.08	3.0	0.07	6.8

Figure 23.   In-Service Eddy Current Inspection Method Results

4.5 CONCLUSIONS

1. The FAI results for pore radius and percent porosity showed a qualitative correlation with X-ray grades for castings that contained gas porosity and shrinkage sponge. By strengthening the data base, it may be possible to use the FAI method to provide quantitative correlations.

2. The FAI technique requires further development before data for foreign materials can be correlated with X-ray results.

3. The accuracy of the FAI percent porosity measurements decreases as the angle between the opposing sides of the specimen increases above about 7°. This may limit the use of the FAI method unless it can be further developed for use with castings that have non-parallel sides.

4. The FAI technique can be used as a pass/fail method for evaluating weld repairs in castings.

5. The in-service eddy current technique can be used successfully for detecting the presence of cracks in component substructure and determining their length.

4.6 RECOMMENDATIONS

1. Maximize the dynamic range of the FAI system to reduce the discrepancies between the data obtained for material of different thicknesses.

2. Use the FAI method to supplement the X-ray and C-scan evaluations in Task 3 to broaden the data base.

3. Use the FAI method as a pass/fail indication for Task 3 weld repair material to supplement X-ray radiography.

4. Improve the capability of the FAI method by using higher resolution scanning, increasing the dynamic range, and/or obtaining a better signal-to-noise ratio.

SECTION 5

PHASE I, TASK 2 - A357-T6 SCREENING TESTS

5.1 INTRODUCTION

The overall Task 2 objective was to define the process variables (solidification rate, aging condition, composition) that provide the optimum balance of tensile and DADT properties of A201-T7 and A357-T6 using screening tests, and to characterize the DADT properties of material produced according to the best process conditions. The screening test data for A357-T6 are discussed in this section. The DADT property characterization will be presented in the next interim report.

Cast plates of A357 (radiographic quality of Grade B, or better) were produced to determine (a) the effect of composition, solidification rate, and aging conditions on DADT properties and (b) if optimization of DADT properties conflicts with the requirements for obtaining the best static (tensile) properties. The range of compositions was based on the AMS specification 4241 [4]. The target tensile properties were 50 ksi UTS, 40 ksi YS, and 3% elongation. Solidification rates and aging parameters were selected to be typical of those used by foundries. The solution heat treatment conditions were maintained constant for all the cast plates.

The screening tests were tension, notched tension, fatigue life, and microstructural analyses. The ratio of the notched tensile strength (NTS) to tensile yield strength (YS) was used as an indicator of fracture toughness. The microstructural analyses included determination of the dendrite arm spacing (DAS), and the size, aspect ratio, and spacing of the silicon particles. The amount of porosity present in each cast plate was also estimated using image analysis.

Multiple regression analyses were conducted to determine the relationships between the process variables, and the mechanical properties and microstructural features.

5.2 EXPERIMENTAL PROCEDURES

5.2.1 Process Variables

Forty-eight A357 plates with variations of composition, solidification rate, and aging parameters were cast by ALCOA. Each plate was 0.75 inch x 6 inches x 12 inches. The same pattern, and gating and risering system shown in Figure 24 were used to produce each plate.

The plates were produced based on the composition specification shown in Figure 25. With the exception of the addition of Sr as a Si particle modifier, the specification is
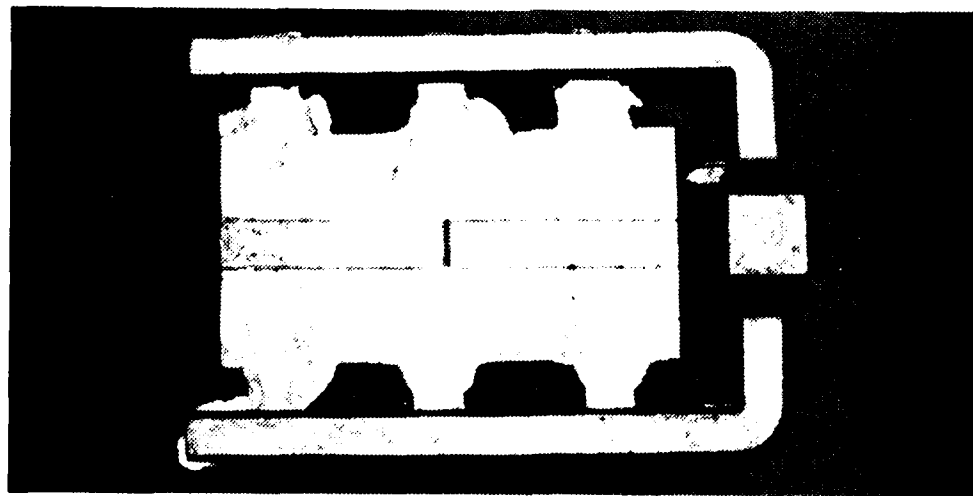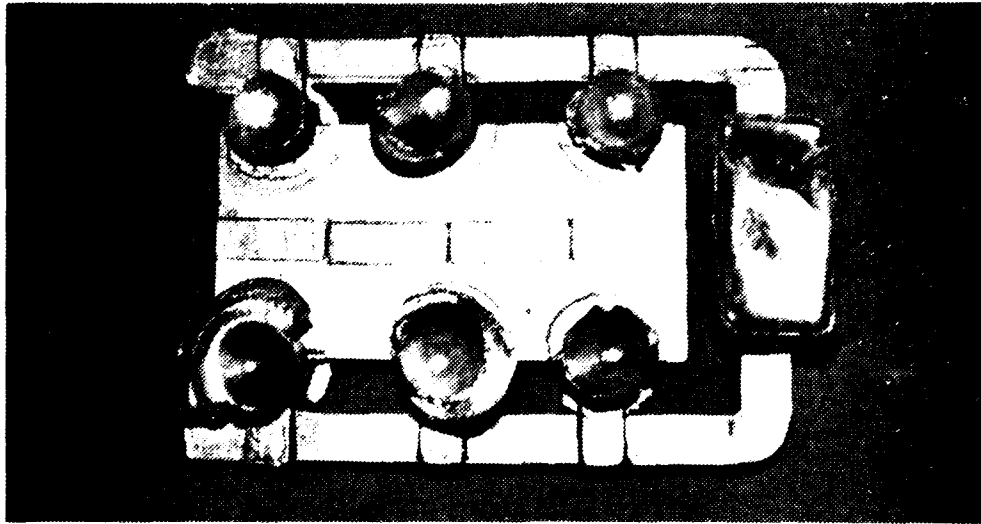
FIGURE 24.   Gating, Risering, and Chill Placement Used for the
              A357 Process Variable Plates

Element[1]	Range (wt %)	
	Min.	Max.
Silicon	6.5	7.5
Magnesium	0.55	0.6
Titanium	0.04	0.20
Beryllium	0.04	0.07
Strontium	0.008	0.016
Iron	—	0.20
Manganese	—	0.10
Others, each	—	0.05
Others, total	—	0.15
Aluminum	Balance	

(1) AMS 4241 (Draft 40GC) plus Sr addition

Figure 25. Composition Specification for the A357-T6 Screening Plates

the same as AMS 4241[4] (Draft 40GC). This initial draft was subsequently modified and approved for general release. The modifications were (a) an increase in the lower limit for Ti from 0.04% to 0.10% and (b) a decrease in the maximum limit for Fe from 0.20% to 0.12%.

The composition of 36 of the 48 plates was varied within the limits allowed by the specification. Due to the number of tests that would be required to evaluate the effect of all the key elements individually, some were grouped together, for example Ti, Mn, and Be. Cast plates were made with close to the minimum or maximum percentages of each element or group of elements. The target for those elements not being specifically varied was the middle of the allowed composition range. The Sr addition was 0.008% to 0.016%, except for those plates where it was specifically omitted. Strontium was included to promote the formation of spheroidal silicon particles in all parts of each plate to improve fatigue properties by reducing the stress concentration associated with irregularly shaped particles.

In addition to the 36 plates that were within the AMS 4241 composition guidelines, 12 plates were made with compositions outside the specification. The composition ranges stipulated in the specification are relatively narrow and, therefore, correlations between properties and alloying element content could be difficult to detect. These additional plates were made to increase the possibility of detecting correlations using regression analyses. A summary of the A357 composition variations evaluated, both within and outside the specification, is shown in Figure 26. Forty-eight combinations of the three process variables (composition, solidification rate, aging parameters) were produced, as shown in Figure 27.

Two solidification rates were achieved by varying the pour temperature and the chill material. Copper or iron chills were placed along the center of the plates (Figure 24) to vary the solidification rate. Pour temperatures of 1380F and 1440F were used with the copper and iron chills, respectively. The solidification rate was not measured directly, but DAS measurements indicated that the plates with the Cu chills had been solidified more rapidly than those with the Fe chills. These plates are referred to as the fast and slow solidification plates in the remainder of this report.

The solution heat treatment parameters were the same for all 48 plates. The plates were heated for 16 hours at 1010 ± 10°F, which is within the requirements of AMS 4241. The plates were quenched in room temperature water with a delay time of less than eight seconds.

The two aging temperature/time combinations were: (a) 315 ± 5F for 12 hours, and (b) 335 ± 5F for 6 hours. These combinations were selected following consultations with several foundries as being representative of the temperature and time

COMPOSITION VARIABLES	COMPOSITION DEVIATION FROM SPECIFICATION MID-RANGE		
	Below Min.	Min.	Max.
Si	(1)	X	X
Mg	X	X	X
Ti, Mn, Be	(1)	X	X
Fe	N/A	(1)	X
Ti	X	(1)	(1)
Fe, Be	X	(1)	(1)
Nominal	Without Sr		
Nominal	With Sr		

(1) Not Evaluated

Figure 26. Composition Variations for the A357-T6 Screening Plates

| Composition[1] | Slow Solidification | | Fast Solidification | |
| | Aging Parameters | | Aging Parameters | |
	315F/12 hrs.	335F/6 hrs.	315F/12 hrs.	335F/6 hrs.
Si				
Max.	X	X	X	X
Min.	X	X	X	X
Mg				
Max.	X	X	X	X
Min.	X	X	X	X
Below Min.	X	X	X	X
Ti, Mn, Be				
Max.	X	X	X	X
Min.	X	X	X	X
Fe				
Max.	X	X	X	X
Ti				
Below Min.	X	X	X	X
Fe, Be				
Below Min.	X	X	X	X
Nominal				
No Sr	X	X	X	X
With Sr	X	X	X	X

(1) Other elements were mid-range of the specification
(2) Each "X" represents one cast plate (total of 48 plates)

Figure 27. A357-T6 Screening Plate Process Variables

ranges typically used for aging A357 castings to the T6 condition. Heat treatment of all the screening plates was conducted by Northrop.

All the A357-T6 castings for screening were Grade B or better according to MIL-A-2175. The plates were radiographically inspected to a 1% sensitivity both by the foundry and subsequently by an independent laboratory. The melt composition of each plate was provided by the foundry and was subsequently verified for each plate by Northrop using inductively coupled plasma (ICP) analysis. The foundry melt analysis is used throughout this report for quoting plate compositions.

5.2.2 Test Procedures

Tension, notched tension, and fatigue life tests were performed in accordance with the ASTM specifications shown in Figure 28. Two specimens per plate were tested for each of these three mechanical properties. The specimens were excised from the same location in each of the 48 plates for consistency. The fatigue specimen, which is shown in Figure 29, is a simple simulation of aircraft components that contain holes for inserting fasteners during aircraft assembly. Holes act as stress concentrators and are a common cause of fatigue problems. All the A357-T6 fatigue specimens were tested to failure using constant amplitude loading, a net maximum tensile stress of 20 ksi, and a stress ratio (R) of 0.1.

5.2.3 Microstructural Characterization

The specific measurements for characterizing the microstructure of each of the 48 plates were: (a) dendrite arm spacing (DAS), (b) silicon particle aspect ratio, area, and spacing, and (c) percent porosity.

The DAS was measured using a line intercept method [5] at the edge and center (under the chill) of each of the 48 plates, and for four of the plates as a function of distance from the center of the plates. The percent porosity was estimated at the center of each plate. The silicon particle morphology was measured at the edge of all 48 plates. The percent porosity and the Si particle morphology were investigated using an Omnicon 3500 Image Analyzer.

5.2.4 Data Analysis

The basic test matrix Figure 27 was completed for each mechanical property and microstructural parameter. For mechanical properties, two tests were averaged for each "X" shown in Figure 27 (a total of 96 tests for each property).

The average properties for the process variables were obtained by averaging the test results for the rows and columns

Test	Specification
Tension	ASTM B557
Notched Tension	ASTM E602
Fatigue Life	ASTM E466

Figure 28. Screening Test Specifications
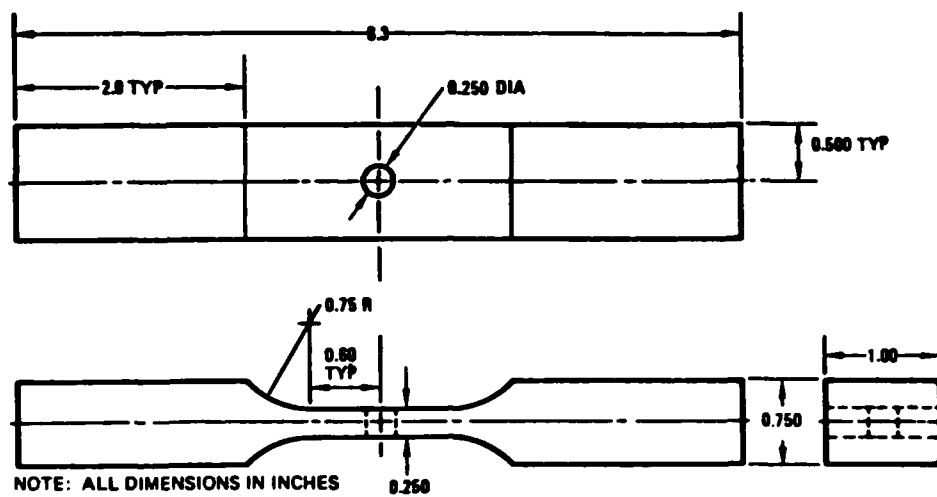
Figure 29. Fatigue Test Specimen

in Figure 27. The general effect of composition was obtained by averaging the data in each row (eight tests per row). The general effects of solidification rate and aging condition were determined by averaging the data in the four columns. For the plates that were within the composition specification, 18 individual test results per column were averaged. An average of six results was obtained per column for the plates that were outside the composition specification.

The plates that were outside the AMS composition specification were made specifically to enhance the regression analyses. All the individual test results for each composition variant shown in Figure 27 were included in the regression analyses. Both linear and nonlinear multiple analyses were conducted. The linear analysis assumed a 5% probability of error for accepting or rejecting a variable in the final relationship, providing a broad indication of the relevant variables before progressing to the nonlinear analysis. The nonlinear analysis is considered to give a more accurate definition of the correlation equation due to its inclusion of cross-product and second order terms. However, the acceptance/rejection criterion was tightened from 5% to 1% probability of error to reduce the number of unrepresentative cross-product items which might otherwise appear in the final equation.

The results of the regression analyses are presented as the percent variation in the dependent variables (mechanical properties and microstructural features) explained by the independent variables (composition, solidification rate, and aging temperature/time).

5.3 RESULTS AND DISCUSSION

The average hardness (Rockwell B) for the plates that were within the composition specification (WCS) was 46 after solution heat treatment and quench (SHT) and 69 after aging. The conductivity values (% of IACS) for these conditions were 34% and 36%, respectively. For the plates that were outside the composition specification (OCS), the hardness of the SHT and the aged plates was 45 and 71, respectively. The corresponding conductivity values were 36% and 39%.

The properties for each plate are presented in the following subsections as a function of the process variables for plates that are (a) within the composition specification, and (b) outside the composition specification. The data are averages of two or more tests.

5.3.1 Composition

The chemical composition of the 12 composition variants was based on the AMS specification shown in Figure 25. Nine of the variants were held within the composition specification; the composition of the other three variants was outside the

54

specification. The average contents of the alloying elements that were specifically controlled are summarized in Figure 30. The target for the elements that were not specifically controlled was the mid-range of the specification.

5.3.2 Microstructure

Dendrite Arm Spacing (DAS)

The DAS results are summarized in Figure 31. For the WCS material, the average DAS at the plate edge and under the chill was 0.0028 inch and 0.0014 inch, respectively. Variations in alloy composition had little effect on the DAS. The average DAS measured at the edge of the plates that were solidified at the faster rate (Cu chill) was slightly smaller than that for the plates solidified at the slower rate (Fe chill), i.e. 0.0027 inch vs. 0.0029 inch. The overall average DAS under both the Cu and Fe chills was the same, i.e. 0.0014 inch. A smaller DAS typically improves mechanical properties [6].

A more detailed determination of the dependence of DAS on distance from the plate center was obtained by measuring the DAS at four locations in each of four WCS plates. These data (Figure 32) showed that DAS increased approximately linearly with distance from the center of the plate, and that the faster solidification rate resulted in a smaller DAS.

The DAS for the OCS plates was similar to those that were within the composition specification. The overall average values for the OCS plates under the chill and at the plate edge were 0.0014 inch and 0.0024 inch, respectively.

Silicon Particle Morphology

The aspect ratio, area, and spacing of the Si particles in each plate were determined using image analysis. The data for all the 48 plates are summarized in Figures 33, 34, and 35, respectively.

(a) Aspect Ratio

For the WCS plates, the overall average aspect ratio was 1.86 and that for the Sr-containing plates (Figure 33) was 1.82. A noticeably higher average aspect ratio of 2.19 was obtained for the plates that did not contain Sr. The average silicon particle aspect ratio of the plates solidified at the faster rate was lower than that of the slow solidification rate material (1.82 vs. 1.90).

For the OCS plates, the overall average aspect ratio was 1.76, which is slightly lower than the value for the WCS plates. No significant effect of solidification rate was observed.

Element	Element (Wt %)						
Content [1]	Si	Mg	Fe	Sr	Ti-Mn-Be	Ti	Fe-Be
Max.	7.41	0.60	0.18	0.016	0.19–0.10–0.053	(2)	(2)
Min.	6.53	0.56	(2)	0.008	0.07–0.00–0.04	(2)	(2)
Below Min.	(2)	0.45	(2)	(2)	(2)	0.00	0.027–0.0005

(1) All other elements were mid-range of the specification.
(2) Not evaluated.

Figure 30. Composition of the A357 Screening Plates

COMPOSITION[1] (Wt. %)	SPECIMEN LOCATION	AVERAGE DAS (10^{-4} IN.)				
		AGE (SLOW SOLIDIFICATION)[2]		AGE (FAST SOLIDIFICATION)[3]		AVERAGE
		315F/12HR	335F/6HR	315F/12HR	335F/6HR	
(a) WITHIN COMPOSITION SPECIFICATION						
0.19Ti-0.10Mn-0.053Be	CHILL	14	17	14	13	15
	EDGE	30	33	29	26	30
0.07Ti-0.00Mn-0.04Be	CHILL	15	13	12	12	13
	EDGE	27	31	28	25	28
0.60Mg	CHILL	14	14	14	14	14
	EDGE	29	28	27	26	28
0.56Mg	CHILL	16	14	12	13	14
	EDGE	28	26	25	25	26
7.41Si	CHILL	13	14	15	14	14
	EDGE	25	24	24	26	25
6.53Si	CHILL	14	13	14	14	14
	EDGE	28	32	30	27	29
0.18Fe	CHILL	13	14	15	16	15
	EDGE	30	31	22	28	28
0.00Sr	CHILL	14	16	13	12	14
	EDGE	30	31	27	27	29
NOMINAL	CHILL	14	15	14	15	14
	EDGE	25	27	24	22	24
AVERAGE	CHILL	14	14	14	14	14
	EDGE	28	30	27	26	28
(b) OUTSIDE COMPOSITION SPECIFICATION						
0.45Mg	CHILL	15	14	13	14	14
	EDGE	20	23	28	25	24
0.00Ti	CHILL	14	21	13	12	15
	EDGE	23	27	23	20	22
0.027Fe-0.0005Be	CHILL	14	17	14	13	14
	EDGE	22	26	28	25	25
AVERAGE	CHILL	14	17	13	13	14
	EDGE	22	25	26	23	24

(1) Other elements; mid-range of the specification.
(2) Fe chill; 1440F pour temperature.
(3) Cu chill; 1380F pour temperature.

Figure 31. Effect of Process Variables on the Dendrite Arm Spacing of A357-T6
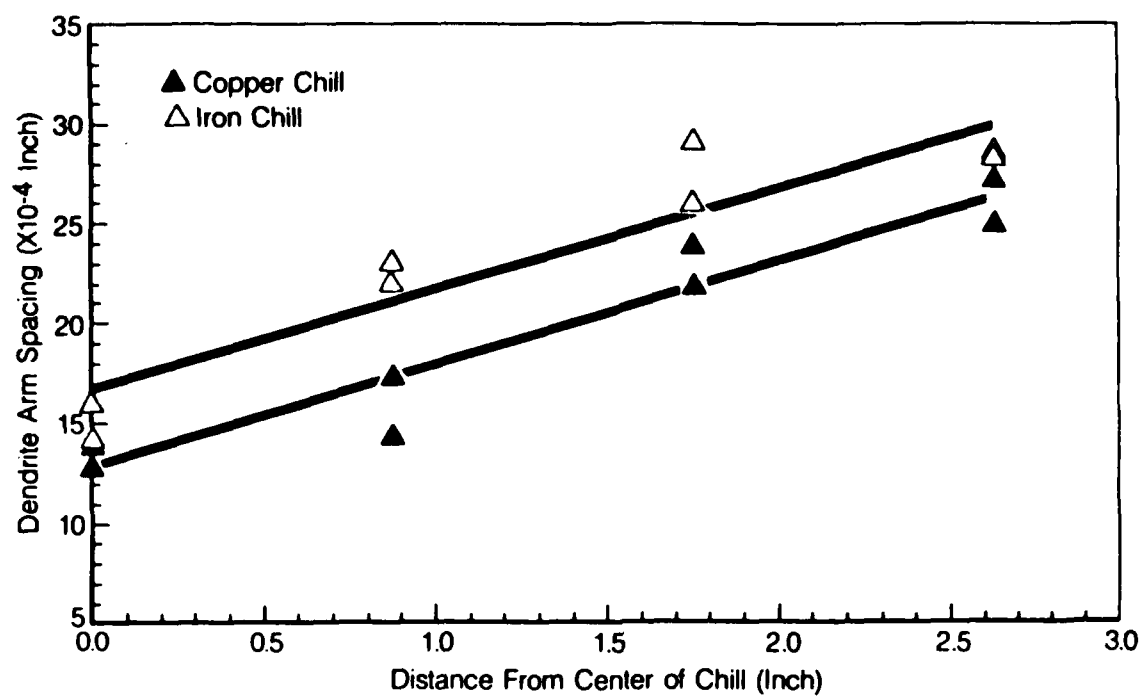
Figure 32.   A357 Dendrite Arm Spacing vs. Distance from the
             Center of the Chill

	SILICON PARTICLE ASPECT RATIO				
COMPOSITION[1] (Wt. %)	AGE (SLOW SOLIDIFICATION)[2]		AGE (FAST SOLIDIFICATION)[3]		AVG.
	315F/12HR	335F/6HR	315F/12HR	335F/6HR	
(a) WITHIN COMPOSITION SPECIFICATION					
0.19Ti-0.11Mn-0.053Be	1.78	1.96	1.74	1.75	1.81
0.07Ti-0.00Mn-0.04Be	1.80	1.70	1.80	1.70	1.75
0.60Mg	1.83	2.00	1.71	1.73	1.82
0.56Mg	1.81	1.80	1.90	1.76	1.82
7.41Si	2.00	1.99	1.80	1.80	1.90
6.53Si	1.92	1.89	1.78	1.73	1.83
0.18Fe	1.73	1.92	1.76	1.89	1.83
0.00Sr	2.06	2.29	2.20	2.19	2.19
NOMINAL	1.77	1.80	1.75	1.75	1.77
AVERAGE	1.86	1.93	1.83	1.81	1.86
(b) OUTSIDE COMPOSITION SPECIFICATION					
0.45Mg	1.72	1.75	1.76	1.76	1.75
0.00Ti	1.77	1.87	1.74	1.74	1.78
0.027Fe-0.0005Be	1.78	1.72	1.81	1.74	1.76
AVERAGE	1.76	1.78	1.77	1.75	1.76

(1) Other elements were mid-range of the specification.
(2) Fe chill; 1440F pour temperature.
(3) Cu chill; 1380F pour temperature.

Figure 33. Effect of Process Variables on the Silicon Particle Aspect Ratio of A357-T6

COMPOSITION [1] (Wt. %)	SILICON PARTICLE AREA (μm^2)				
	AGE (SLOW SOLIDIFICATION) [2]		AGE (FAST SOLIDIFICATION) [3]		AVG.
	315F/12HR	335F/6HR	315F/12HR	335F/6HR	
(a) WITHIN COMPOSITION SPECIFICATION					
0.19Ti-0.11Mn-0.053Be	16	21	19	16	18
0.07Ti-0.00Mn-0.04Be	21	20	18	15	18
0.60Mg	25	19	18	19	20
0.56Mg	17	24	14	15	18
7.41Si	18	21	20	19	19
6.53Si	23	22	23	19	22
0.18Fe	18	32	18	24	23
0.00Sr	83	108	66	70	82
NOMINAL	20	27	19	22	22
AVERAGE	27	33	24	24	27
(b) OUTSIDE COMPOSITION SPECIFICATION					
0.45Mg	16	18	19	17	17
0.00Ti	19	23	19	18	20
0.027Fe-0.0005Be	16	18	22	19	19
AVERAGE	17	19	20	18	19

(1) Other elements were mid-range of the specification.
(2) Fe chill; 1440F pour temperature.
(3) Cu chill; 1380F pour temperature.

Figure 34.   Effect of Process Variables on the Silicon Particle
Area of A357-T6

| COMPOSITION[1] (Wt. %) | SILICON PARTICLE SPACING (μm) | | | | |
| | AGE (SLOW SOLIDIFICATION)[2] | | AGE (FAST SOLIDIFICATION)[3] | | AVG. |
	315F/12HR	335F/6HR	315F/12HR	335F/6HR	
(a) WITHIN COMPOSITION SPECIFICATION					
0.19Ti-0.11Mn-0.053Be	38	34	29	33	34
0.07Ti-0.00Mn-0.04Be	42	34	36	32	36
0.60Mg	44	37	44	40	41
0.56Mg	41	34	30	32	34
7.41Si	40	41	41	43	41
6.53Si	30	28	39	34	33
0.18Fe	29	35	34	38	34
0.00Sr	76	64	59	63	66
NOMINAL	53	51	39	53	49
AVERAGE	44	40	39	41	41
(b) OUTSIDE COMPOSITION SPECIFICATION					
0.45Mg	35	45	35	47	41
0.00Ti	47	57	42	42	47
0.027Fe-0.0005Be	37	44	41	49	43
AVERAGE	40	49	39	46	44

(1) Other elements were mid-range of the specification.
(2) Fe chill; 1440F pour temperature.
(3) Cu chill; 1380F pour temperature.

Figure 35. Effect of Process Variables on the Silicon Particle Spacing of A357-T6

(b) <u>Area</u>

The overall average Si particle area (Figure 34) was
27 μm^2. The average for the WCS Sr-containing variants was
20 μm^2 and showed only minor variations due to composition
changes. The average Si particle area in the Sr-free plates,
however, was over four times greater than that of the plates that
contained Sr (82 μm^2 vs. 20 μm^2).

The effect of solidification rate on aspect ratio was much
greater for the Sr-free than for the Sr-containing plates. The
average Si particle area for plates without Sr that were
solidified at the faster and slower rates was 68 and 95 μm^2,
respectively. For plates containing Sr, the values were 19 and
21 μm^2, respectively.

The average Si particle area determined for the OCS plates
was 19 μm^2. There was no significant effect of solidification
rate or composition. The results were essentially the same as
those for the WCS Sr-containing plates.

(c) <u>Spacing</u>

The overall average Si particle spacing for the WCS plates
was 41 μm (Figure 35). The average Si particle spacing for the
Sr-containing variants and those that did not contain Sr was
36 μm and 66 μm, respectively. For the Sr-free plates, the
faster solidification rate (Cu chill) produced a slightly smaller
average spacing than that for the material solidified slowly (Fe
chill), 61 μm vs. 70 μm. No effect of solidification rate was
observed for the Sr-containing plates.

The average spacing for the OCS plates was 44 μm, i.e.
slightly higher than the WCS material (41 μm). The average
values for the slow and fast solidification rates were 44.5 μm
and 42.5 μm, respectively.

The effect of Sr content on the Si particle aspect ratio,
area, and spacing is illustrated in Figure 36. The
photomicrographs are typical of material taken from the edge of
the plate. The Si particles of the Sr-free material are larger,
more irregularly shaped, and are spaced further apart compared
with those observed in the Sr-containing material. Large,
irregularly shaped particles of the type seen in the material
without Sr can be detrimental to DADT properties, particularly
fatigue crack initiation [7,8].

Though the Sr modified the Si particles, there was no effect
on DAS (Figure 31). For material under the chill, the Si
particle morphology was equivalent for both the solidification
rates. However, the addition of a modifier such as Sr will
ensure that an optimum Si particle morphology can be obtained in
all parts of a casting, including those that are not under or
near a chill. This may be particularly important for DADT
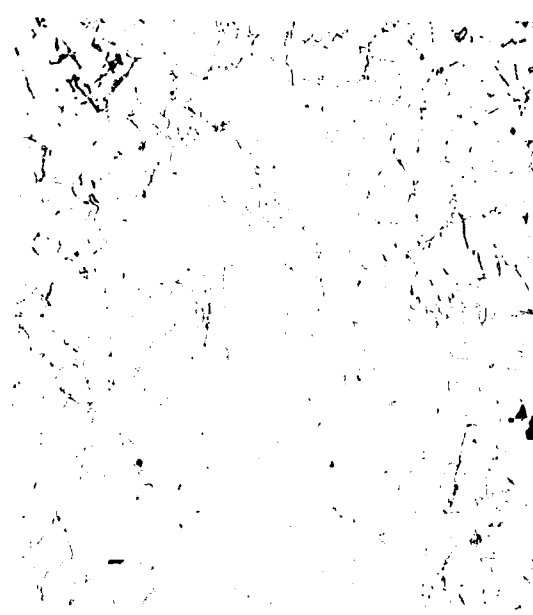
50X   50X
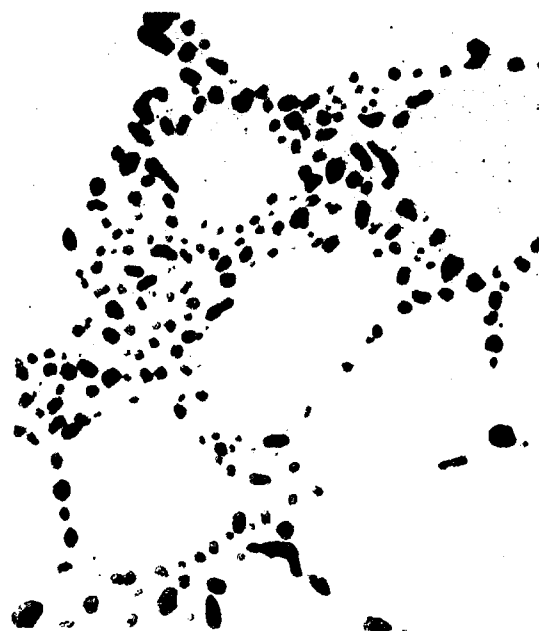
400X   400X

(a) 0.010% Sr   (b) 0.0% Sr

Figure 36.   Effect of Strontium on the A357-T6 Microstructure

properties, which may be more sensitive to Si particle morphology than static properties.

The mechanism by which Sr modifies the Si particle morphology is not fully understood, although several possible explanations have been described [9]. Sr may change the equilibrium at the solid-liquid interface due to solute build-up, producing a hard-to-detect ternary phase. Sr may also change the nucleation kinetics and inhibit growth of the Si particles on the preferred [111] plane.

Percent Porosity

The percent porosity for each plate was estimated using image analysis. The data were obtained from specimens taken from the center of the plate under the chill. Each result presented is the average of about 50 fields of view within the microstructure specimen. The data are summarized in Figure 37.

For the WCS plates, the average porosity of the material solidified at the slower rate (Fe chill) was about three times that of the fast solidification material (Cu chill). This is probably due to the increased time available for dissolution of hydrogen from the melt at the slower solidification rate [9] and/or a greater hydrogen content in the higher temperature melt. However, even with the same melt gas content, a slower solidification rate would tend to promote the formation of more gas porosity than that for material solidified more rapidly. The actual hydrogen content of the melt was not determined, but bubbles were not detected in the vacuum test samples from either of the melts. The other process variables had no effect on the percent porosity. X-ray inspection showed all plates to be Grade B or better.

All the OCS plates were also Grade B, or better, according to X-ray radiography. Unlike the WCS plates, no significant effect of solidification rate on the percent porosity was observed. Only two of the 12 plates contained a detectable amount of porosity (one each for slow and fast solidification rate material).

5.3.3 Tensile Properties

The tensile property data are summarized in Figures 38, 39, and 40 for the plates that were within and outside the composition specification. The overall average tensile properties are shown below:

COMPOSITION[1] (Wt. %)	PERCENT POROSITY				
	AGE (SLOW SOLIDIFICATION)[2]		AGE (FAST SOLIDIFICATION)[3]		AVG.
	315F/12HR	335F/6HR	315F/12HR	335F/6HR	
(a) WITHIN COMPOSITION SPECIFICATION					
0.19Ti-0.11Mn-0.053Be	0.030	0.040	0.001[4]	0.001	0.018
0.07Ti-0.00Mn-0.04Be	0.050	0.001	0.030	0.010	0.023
0.60Mg	0.040	0.020	0.001	0.040	0.025
0.56Mg	0.010	0.001	0.001	0.001	0.003
7.41Si	0.001	0.070	0.030	0.060	0.040
6.53Si	0.060	0.010	0.001	0.020	0.023
0.18Fe	0.050	0.010	0.001	0.001	0.016
0.00Sr	0.050	0.030	0.001	0.001	0.021
NOMINAL	0.001	0.030	0.001	0.001	0.010
AVERAGE	0.047	0.024	0.007	0.015	0.023
(b) OUTSIDE COMPOSITION SPECIFICATION					
0.45Mg	0.001	0.001	0.001	0.110	0.028
0.00Ti	0.001	0.030	0.001	0.001	0.008
0.027Fe-0.0005Be	0.001	0.001	0.001	0.001	0.001
AVERAGE	0.001	0.011	0.001	0.037	0.012

(1) Other elements were mid-range of the specification.
(2) Fe chill; 1440F pour temperature.
(3) Cu chill; 1380F pour temperature.
(4) No porosity detected - below the detection limit of the equipment

Figure 37. Effect of Process Variables on the Percent Porosity of A357-T6

COMPOSITION[1] (Wt. %)	AVERAGE ULTIMATE TENSILE STRENGTH (ksi)				
	AGE (SLOW SOLIDIFICATION)[2]		AGE (FAST SOLIDIFICATION)[3]		AVG.
	315F/12HR	335F/6HR	315F/12HR	335F/6HR	
(a) WITHIN COMPOSITION SPECIFICATION					
0.19Ti-0.10Mn-0.053Be	50.4	50.3	51.2	53.4	51.3
0.07Ti-0.00Mn-0.04Be	49.0	51.8	49.1	54.2	51.0
0.60Mg	49.7	51.8	52.0	54.6	52.0
0.56Mg	50.1	52.1	53.5	54.1	52.5
7.41Si	49.5	51.4	51.0	51.8	50.9
6.53Si	49.8	53.2	51.6	51.4	51.5
0.18Fe	50.0	51.2	52.2	52.0	51.4
0.00Sr	49.6	51.2	52.5	52.7	51.5
NOMINAL	51.5	49.5	50.7	51.4	50.8
AVERAGE	50.0	51.4	51.5	52.8	51.4
(b) OUTSIDE COMPOSITION SPECIFICATION					
0.45Mg	50.6	51.8	50.5	49.0	50.5
0.00Ti	51.0	48.9	52.0	51.5	50.9
0.027Fe-0.0005Be	52.5	51.8	49.0	52.3	51.4
AVERAGE	51.4	50.8	50.5	51.0	50.9

(1) Other elements were mid-range of the specification
(2) Fe chill; 1440F pour temperature
(3) Cu chill; 1380F pour temperature

Figure 38. Effect of Process Variables on the Ultimate Tensile Strength of A357-T6

| COMPOSITION[1] (Wt. %) | AVERAGE YIELD STRENGTH (ksi) | | | | |
| | AGE (SLOW SOLIDIFICATION)[2] | | AGE (FAST SOLIDIFICATION)[3] | | AVG. |
	315F/12HR	335F/6HR	315F/12HR	335F/6HR	
(a) WITHIN COMPOSITION SPECIFICATION					
0.19Ti-0.10Mn-0.053Be	42.1	43.6	41.8	44.5	43.0
0.07Ti-0.00Mn-0.04Be	41.9	43.8	41.6	44.6	43.0
0.60Mg	41.2	44.7	43.1	45.7	43.7
0.56Mg	42.0	43.9	42.8	45.8	43.6
7.41Si	41.9	44.5	41.8	44.0	43.0
6.53Si	41.6	44.7	42.0	43.8	43.0
0.18Fe	42.8	45.2	43.3	45.0	44.1
0.00Sr	42.5	45.5	43.0	44.3	43.8
NOMINAL	42.8	42.4	41.6	45.1	43.0
AVERAGE	42.1	44.2	42.3	44.8	43.4
(b) OUTSIDE COMPOSITION SPECIFICATION					
0.45Mg	40.1	42.8	38.9	41.0	40.7
0.00Ti	41.8	41.8	42.0	43.2	42.2
0.027Fe-0.0005Be	42.8	44.9	42.8	44.4	43.7
AVERAGE	41.6	43.2	41.2	42.9	42.2

(1) Other elements were mid-range of the specification
(2) Fe chill; 1440F pour temperature
(3) Cu chill; 1380F pour temperature

Figure 39. Effect of Process Variables on the Yield Strength of A357-T6

COMPOSITION[1] (Wt. %)	AVERAGE ELONGATION (%)				
	AGE (SLOW SOLIDIFICATION)[2]		AGE (FAST SOLIDIFICATION)[3]		AVG.
	315F/12HR	335F/6HR	315F/12HR	335F/6HR	
(a) WITHIN COMPOSITION SPECIFICATION					
0.19Ti-0.10Mn-0.053Be	5.2	1.5	6.5	6.8	5.0
0.07Ti-0.00Mn-0.04Be	4.0	5.0	3.5	9.2	5.4
0.60Mg	4.5	4.2	6.0	7.0	5.4
0.56Mg	4.6	5.5	9.5	7.0	6.7
7.41Si	4.0	3.2	6.8	5.2	4.8
6.53Si	5.1	6.0	9.0	5.7	6.5
0.18Fe	3.2	3.0	5.2	5.2	4.2
0.00Sr	2.5	1.8	5.5	4.2	3.5
NOMINAL	5.8	4.1	5.3	3.6	4.7
AVERAGE	4.3	3.8	6.4	6.0	5.1
(b) OUTSIDE COMPOSITION SPECIFICATION					
0.45Mg	11.2	7.6	13.6	6.3	9.7
0.00Ti	6.0	3.2	7.2	6.7	5.8
0.027Fe-0.0005Be	10.9	6.8	10.1	5.6	8.3
AVERAGE	9.3	5.9	10.3	6.2	7.9

(1) Other elements were mid-range of the specification
(2) Fe chill; 1440F pour temperature
(3) Cu chill; 1380F pour temperature

Figure 40.   Effect of Process Variables on the Elongation of A357-T6

	UTS (ksi)	YS (ksi)	El (%)
Within Composition Specification	51.4	43.4	5.1
Outside Composition Specification	50.9	42.2	7.9

The average ultimate and yield strengths for the two groups of material were very similar, though the elongation of the OCS material was higher than that of the WCS material. The results are discussed in more detail below.

Ultimate Tensile Strength

The UTS (Figure 38) was not significantly affected by any of the composition variants. A slightly higher value was obtained for the WCS plates solidified at the faster rate compared with those solidified more slowly, i.e. 52.2 ksi vs. 50.7 ksi. A slightly higher UTS (52.1 ksi) was obtained for the WCS variants that were aged at 335F for 6 hours compared with those that were aged at 315F for 12 hours (50.7 ksi).

The UTS of the OCS plates was not significantly affected by aging conditions, solidification rate, or composition.

In summary, the UTS (WCS plates) was only slightly influenced by solidification rate and aging procedures.

Tensile Yield Strength

Similar to the UTS, the yield strength (Figure 39) was not significantly affected by composition. On average, the WCS plates had a slightly higher yield strength than the OCS plates (43.4 ksi vs 42.2 ksi, respectively). The variant that differed most from the overall average value was the low Mg (0.45%) variant (OCS), with a yield strength of 40.7 ksi. The solidification rate did not affect the yield strength of either the WCS or the OCS plates.

The aging conditions had the most significant effect on yield strength. The material aged at 335F for 6 hours had a higher yield strength than that aged at 315F for 12 hours. For the WCS plates the averages were 44.5 ksi and 42.2 ksi, respectively. For the OCS plates, the yield strength values were 43.0 ksi and 41.4 ksi, respectively.

In summary, the yield strength was influenced mainly by the aging conditions. The OCS plates had a slightly lower yield strength than those that were within the composition specification.

Elongation

The composition had a greater effect on elongation to failure (Figure 40) than it had on either the ultimate or the yield strengths. The WCS variants that did not contain Sr had the lowest average value (3.5%). The OCS plates had the highest elongation, particularly the low Mg (9.7%) and the low Fe/Be (8.3%) variants.

The plates that were solidified at the faster rate had an average elongation of 6.2% (WCS) and 8.2% (OCS). For the WCS plates, the elongation for the rapidly solidified material was higher (6.2%) than those that were solidified more slowly (4.0%). For the OCS plates, the difference in elongation due to solidification rate was not significant (7.8% and 8.2% for the slow and fast solidification rate plates, respectively).

For the WCS plates, the aging conditions had no affect on the average elongation. The values were 5.3% and 4.9% for the 315F/12 hour and 335F/6 hour combinations, respectively. For the OCS plates, the average elongation for the 335F/6 hour aging combination plates was 6.0%, compared with 9.8% for those that were aged at 315F for 12 hours.

In summary, composition, solidification rate, and aging conditions (OCS plates only) all influenced the elongation to failure.

5.3.4 Notched Tensile Strength and NTS/YS Ratio

The average NTS and NTS/YS ratio data for each plate are shown in Figures 41 and 42, respectively. The overall average NTS values for WCS and OCS material are 52.5 ksi and 54.9 ksi, respectively. The corresponding NTS/YS ratios are 1.21 and 1.30.

The Sr-free plates had a significantly lower NTS (44.1 ksi) than any other composition variant. The Sr-free material also had by far the lowest NTS/YS ratio (1.01). The modified Si particle morphology, which is due to the presence of Sr, clearly has a beneficial affect on the NTS and the NTS/YS ratio, indicating that Sr should significantly improve fracture toughness. The effect of Sr on Si particle morphology was shown in Figure 36. The effect of Sr on the NTS/YS ratio is plotted in Figure 43 for the WCS plates and shows that the highest NTS/YS ratio was obtained for material that contained about 0.013% Sr.

The low Fe/Be OCS variant had the highest NTS (58.5 ksi) and a NTS/YS ratio (1.34) that was significantly higher than the average value for the WCS material (1.21). The highest NTS/YS ratio (1.37) was obtained for the OCS low Mg material. These results indicate that the low OCS Fe/Be and Mg variants should

COMPOSITION[1] (Wt. %)	AVERAGE NOTCHED TENSILE STRENGTH (ksi)				
	AGE (SLOW SOLIDIFICATION)[2]		AGE (FAST SOLIDIFICATION)[3]		AVG.
	315F/12HR	335F/6HR	315F/12HR	335F/6HR	
(a) WITHIN COMPOSITION SPECIFICATION					
0.19Ti-0.10Mn-0.053Be	51.9	48.4	56.0	56.9	53.3
0.07Ti-0.00Mn-0.04Be	55.7	53.6	55.2	58.9	55.9
0.60Mg	51.6	53.9	56.0	56.9	54.6
0.56Mg	48.8	54.4	57.7	58.1	54.7
7.41Si	51.1	52.2	53.0	50.0	51.6
6.53Si	48.8	50.8	55.2	56.0	52.7
0.18Fe	52.8	48.6	53.8	52.3	51.9
0.00Sr	43.2	42.7	46.0	44.4	44.1
NOMINAL	55.9	52.4	55.8	49.8	53.5
AVERAGE	51.1	50.8	54.3	53.7	52.5
(b) OUTSIDE COMPOSITION SPECIFICATION					
0.45Mg	58.0	55.1	56.0	52.9	55.5
0.00Ti	52.9	44.9	51.2	54.1	50.8
0.027Fe-0.0005Be	61.2	57.0	57.5	58.0	58.5
AVERAGE	57.4	52.4	54.9	55.0	54.9

(1) Other elements were mid-range of the specification
(2) Fe chill; 1440F pour temperature
(3) Cu chill; 1380F pour temperature

Figure 41. Effect of Process Variables on the Notched Tensile Strength of A357-T6

COMPOSITION[1] (Wt. %)	AVERAGE NTS/YS RATIO				
	AGE (SLOW SOLIDIFICATION)[2]		AGE (FAST SOLIDIFICATION)[3]		AVG.
	315F/12HR	335F/6HR	315F/12HR	335F/6HR	
(a) WITHIN COMPOSITION SPECIFICATION					
0.19Ti-0.10Mn-0.053Be	1.23	1.11	1.34	1.28	1.24
0.07Ti-0.00Mn-0.04Be	1.33	1.22	1.33	1.32	1.30
0.60Mg	1.26	1.21	1.30	1.25	1.25
0.56Mg	1.16	1.24	1.35	1.26	1.25
7.41Si	1.22	1.17	1.27	1.14	1.20
6.53Si	1.17	1.14	1.32	1.27	1.22
0.18Fe	1.24	1.08	1.24	1.16	1.18
0.00Sr	1.02	0.94	1.07	1.00	1.01
NOMINAL	1.31	1.24	1.34	1.11	1.25
AVERAGE	1.21	1.15	1.28	1.20	1.21
(b) OUTSIDE COMPOSITION SPECIFICATION					
0.45Mg	1.45	1.29	1.44	1.29	1.37
0.00Ti	1.26	1.07	1.22	1.25	1.20
0.027Fe-0.0005Be	1.43	1.27	1.35	1.31	1.34
AVERAGE	1.38	1.21	1.33	1.28	1.30

(1) Other elements were mid-range of the specification
(2) Fe chill; 1440F pour temperature
(3) Cu chill; 1380F pour temperature

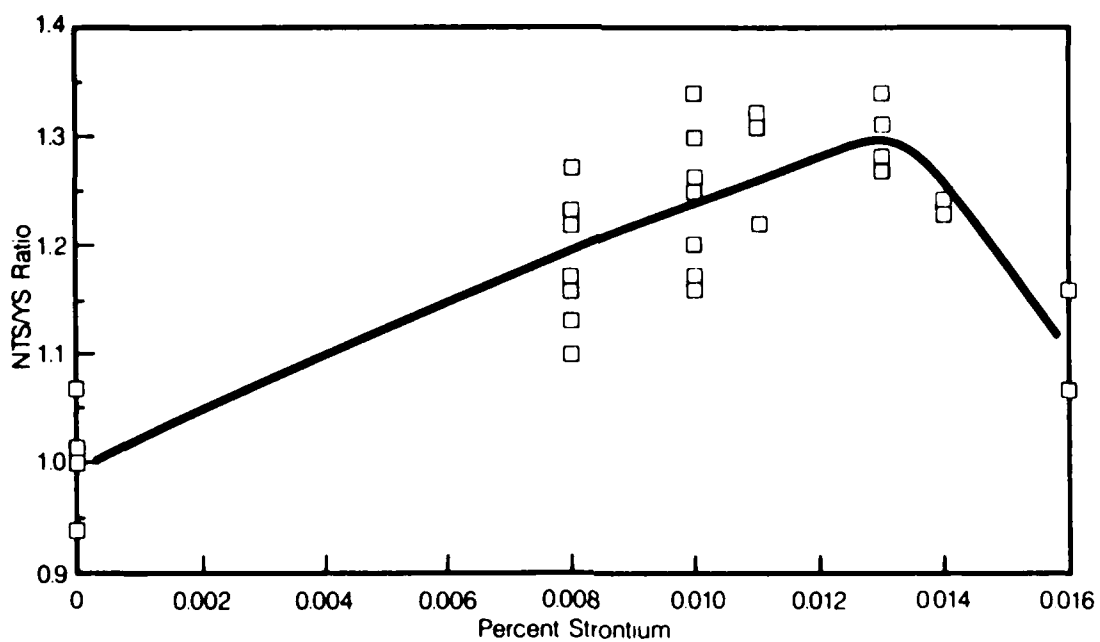Figure 42. Effect of Process Variables on the NTS/YS Ratio of A357-T6

Figure 43.   A357-T6 NTS/YS Ratio Vs. Percent Strontium for Plates
That Were Within the Composition Specification.

73

each have excellent fracture toughness, which is consistent with the excellent ductility obtained for both variants.

The solidification rate also influenced both the NTS and the NTS/YS ratio. For the WCS plates, the NTS averaged 54 ksi and 51 ksi for the fast and slow solidification rates, respectively. For the OCS variants, the average NTS was the same for both solidification rates, about 55 ksi. The NTS/YS ratio was 1.24 for the fast solidification rate WCS material, compared with 1.18 for the slow solidification rate material. For the OCS variants, the NTS/YS ratio was the same (1.30) for the two solidification rates.

The aging conditions did not influence the NTS of the WCS material. The NTS for the 315F/12 hour combination was, however, higher than the 335F/6 hour material for the OCS variants, 56.1 ksi vs 53.7 ksi. The NTS/YS ratio was slightly higher for the 315F/12 hour aging condition than for the 335F/6 hour age for both the WCS (1.24 and 1.17) and the OCS (1.35 and 1.24) variants. The variations in the NTS/YS ratio were due to the change in yield strength with aging condition.

In summary, NTS and NTS/YS ratio improvements were obtained by including Sr to modify the Si particle morphology. The fast solidification rate was also beneficial, compared with the slower rate. Low levels of Mg and Fe/Be in specific OCS plate variants resulted in high NTS and NTS/YS ratio values.

5.3.5 Fatigue Life

The fatigue life data are summarized in Figure 44 for plates that were both within and outside the composition specification. All the data in Figure 44 are log averages of the fatigue life results for each plate. At least two specimens were tested for each plate. Additional tests were conducted where a considerable discrepancy between the two test results was obtained. All fatigue tests were conducted at constant amplitude using a net maximum stress of 20 ksi, and an R ratio of 0.1.

Significant scatter of the fatigue life data for individual specimens was obtained, which is typical for most materials. The precise location of casting defects in the specimen would influence fatigue life, which would be shorter if the defects were located near the area of peak stress (near the hole). The overall averages were 131×10^3 and 66×10^3 cycles to failure for the WCS and OCS materials, respectively. There were differences in fatigue life between the composition variants that were at the maximum and minimum composition limits for a given alloying element or group of elements. However, because of the significant scatter in the results, differences in the average fatigue life values for the compositional variants shown in Figure 44 were considered to be insignificant.

74

	LOG AVERAGE FATIGUE LIFE (10^3 CYCLES TO FAILURE)*				
COMPOSITION[1]	AGE (SLOW SOLIDIFICATION)[2]		AGE (FAST SOLIDIFICATION)[3]		AVERAGE
	315F/12HR	335F/6HR	315F/12HR	335F/6HR	
(a) WITHIN COMPOSITION SPECIFICATION					
0.19Ti-0.10Mn-0.053Be	98	104	193	222	149
0.07Ti-0.00Mn-0.04Be	168	136	163	199	165
0.60Mg	78	102	373	165	150
0.56Mg	145	86	620	523	189
7.41Si	66	59	117	58	76
6.53Si	94	131	103	92	104
0.18Fe	70	84	102	350	118
0.00Sr	53	75	175	79	99
NOMINAL	57	66	40	44	51
LOG AVERAGE	85	90	156	144	131
(b) OUTSIDE COMPOSITION SPECIFICATION					
0.45Mg	78	59	88	56	69
0.00Ti	78	54	56	71	64
0.027Fe-0.0005Be	82	73	53	54	64
LOG AVERAGE	79	62	64	60	66

*Specimen with a hole; Kt=2.42; net maximum stress=20 ksi
(1) Other elements were mid-range of the specification.
(2) Fe chill; 1440F pour temperature.
(3) Cu chill; 1380F pour temperature.

Figure 44.   Effect of Process Variables on the Fatigue Life
             of A357-T6

The WCS material that was solidified at the faster rate had a longer average fatigue life (150 x 10^3 cycles) compared with that for the slow solidification rate material (88 x 10^3). This higher average fatigue life is attributed to a lower percentage porosity in these plates (0.011%) compared with the material solidified more slowly (0.035%) as shown in Figure 37. Fatigue cracks typically initiate at pores in casting alloys [10].

No significant effect of aging conditions on the fatigue life of the WCS variants was apparent.

Even considering the large amount of scatter in the data, the average fatigue life for the OCS plates (66 x 10^3 cycles to failure) was significantly shorter than that of the WCS plates. No significant effects of composition, solidification rate, or aging conditions were observed.

In summary, the fatigue life of the WCS A357-T6 appears to be related to the percent porosity, even though all the plates were Grade B, or better.

5.3.6 Regression Analysis

Linear and nonlinear regression analyses were conducted as described in Section 5.2.4. The results are summarized in Figure 45. The percent variation in each dependent variable (e.g. mechanical property) explained by the independent variables in the linear analysis (e.g. composition) are listed. The individual contributions of the independent variables in the nonlinear analysis are not shown because they cannot be defined due to the cross-correlation terms generated. However, the total contribution of the relevant variables is listed. In general, the results of the regression analyses support the overall trends observed from the data discussed in previous subsections.

The effect of aging condition consisted of concurrently varying temperature and time and is represented in the regression analyses only by the aging temperature for the two temperature/time combinations evaluated (335F/6 hrs and 315F/12 hrs). The solidification rate was represented by the average DAS for the fast (0.0021 inch) and slow (0.0024 inch) rates at a point midway between the center and edge of the plate (Figure 32).

All the WCS and OCS data were included in the data set. The results for the linear and nonlinear analyses are discussed separately below.

Linear Analysis

The criterion used to accept or reject the contribution of an independent variable to the variation of the dependent variable was a 5% probability of error. This large percentage was chosen so that the best indication of the contributing variables could be determined.

	LINEAR ANALYSIS(1)										NONLINEAR ANALYSIS(2)
	PERCENT VARIATION EXPLAINED BY PROCESS VARIABLES									TOTAL PERCENT VARIATION EXPLAINED	TOTAL PERCENT VARIATION EXPLAINED
PROPERTY	AGING PARAMETERS	SOLIDIFICATION RATE	Mg	Sr	Fe	Be	Si	Mn			
UTS	12	13	–	–	–	–	–	–		25	0
YS	50	–	15	–	14	5	–	–		84	77
EL	–	13	25	–	–	–	–	–		38	60
NTS	–	–	–	37	–	7	–	–		44	84
NTS/YS	16	–	8	31	13	–	–	–		68	78
FATIGUE LIFE	–	11	–	–	9	–	–	–		20	57
DAS(3)	–	–	–	–	–	–	11	22		33	47
PERCENT POROSITY	–	–	–	–	–	–	–	–		0	14
Si PARTICLE AREA	–	–	–	55	4	–	6	–		65	92
Si PARTICLE ASPECT RATIO	–	–	–	52	8	–	4	–		64	76
Si PARTICLE SPACING	–	–	–	32	–	–	–	14		46	68

(1) 5% error level
(2) 1% error level
(3) At the edge of the plate

Figure 45. Linear and Nonlinear Regression Analysis Results for A357–T6

The dependent variables with the largest explained variations were yield strength, NTS, NTS/YS ratio, and Si particle size area, spacing, and aspect ratio. With the exception of yield strength, the Sr content had the most significant effect on these parameters. The yield strength was primarily influenced by the aging parameters (50%) with smaller contributions from Mg (15%) and Fe (14%).

Other significant contributions to the variation in the dependent variables were elongation (25% - Mg), and DAS at the edge of the plate (22% - Mn). The relationship observed earlier (Section 5.3.2) between solidification rate and percent porosity was not confirmed by the regression analysis.

Nonlinear Analysis

A tighter acceptance/rejection criterion of 1% was used in this analysis. Despite this fact, the total percentage variation explained by the nonlinear analysis was usually greater than that determined by the linear analysis. If the nonlinear percentage is lower but similar to the linear value, a linear relationship is indicated. If the nonlinear percentage is greater than the linear percentage, the increase is due to the inclusion of second-order and/or cross-product terms. For example, the total percent variation in the NTS/YS ratio increased from 68% (linear analysis) to 78% (nonlinear analysis). By plotting the data (Figure 43), it was shown that a nonlinear relationship existed between the NTS/YS ratio and the Sr content.

Other increases in the total percent variation explained were noted for elongation, NTS, fatigue life, DAS, and Si particle area, aspect ratio, and spacing, indicating nonlinear relationships.

The UTS showed a reduction in the percent variation explained from 25% (linear) to 0% (nonlinear). This reduction is probably due to the tighter (1%) error level for the nonlinear analysis and the fact that the linear correlation was relatively weak. For the percent porosity, the percent variation explained increased from 0% (linear) to 14% (nonlinear). Even the latter is too small to indicate a significant correlation between percent porosity and any of the independent variables.

5.4 CONCLUSIONS

The combined conclusions from both the tabulated data and the regression analyses regarding the effect of process variables on the mechanical properties and microstructural features of A357-T6 are as follows:

1. **Composition**

   o The addition of Sr improved:
   - Si particle morphology of material that was not under the chill
   - NTS and NTS/YS ratio (up to 0.013% Sr)
   - ductility
   o Low Fe/Be and Mg material (OCS) had the highest ductilities and NTS/YS ratios
   o Low Fe/Be material (OCS) had the highest NTS
   o Low (OCS) Mg material had the lowest yield strength and highest ductility.

2. **Solidification Rate**

   o Faster solidification rates (Cu chill) improved ultimate strength, ductility, NTS, NTS/YS ratio, and the fatigue life of the WCS plates.
   o There was no significant effect of solidification rate on the properties of OCS plates.

3. **Aging Temperature/Time**

   o The yield strength was higher for the 335F/6 hrs aging condition than for 315F/12 hrs (WCS and OCS plates).
   o Ductility, NTS, and the NTS/YS ratio were higher for the OCS plates that were aged at 315F for 12 hours than those aged at 335F for 6 hours.

4. **Property Optimization**

   The requirements for optimizing the DADT and tensile properties of A357-T6 do not conflict.

5.5 **RECOMMENDATIONS**

1. The approved AMS 4241 specification, with the addition of a Si modifier, such as Sr, should be used for producing the A357-T6 verification plates for the remaining portion of Task 2, Phase I, and for the remainder of the DADTAC program.

2. The plates for subsequent characterization of DADT properties should be solidified at a rate fast enough to maintain the DAS below 0.0024 inch in designated areas.

79

SECTION 6

PHASE I, TASK 2 - A201-T7 SCREENING TESTS

6.1 INTRODUCTION

The overall objective, procedures, and test methods for the A201-T7 screening test subtask were the same as those described in Section 5.1 for A357-T6. The composition for the cast plates was based on the AMS 4242 specification [11]. The target tensile properties were 60 ksi UTS, 50 ksi YS, and 3% elongation. Only the within composition specification (WCS) data are reported for A201-T7. The testing of the plates that were outside the composition specification (OCS) was incomplete at the time of writing this report and will be included in the next interim report.

6.2 EXPERIMENTAL PROCEDURES

6.2.1 Process Variables

Twenty cast plates with variations of composition, solidification rate, and aging parameters were produced by Hitchcock Industries. Each plate was 0.75-inch-thick x 6-inches-wide x 12-inches-long. The same pattern, and gating and risering systems were used to produce each plate. Figure 46 shows the orientation of the gates, risers, and chills (drag only) used to produce these plates.

The plates were produced using the composition specification AMS 4242 (Draft 40GD), which is shown in Figure 47. This initial draft was subsequently modified and approved for general release. The modifications were (a) a change in the range for Ag from 0.5-1.0% to 0.4-0.8% and (b) the Mg range was changed from 0.25-0.35% to 0.20-0.30%.

A summary of the A201 composition variations evaluated is shown in Figure 48.

The composition of all the plates was varied within the draft AMS specification. It was not possible to vary all the key elements individually; Ti-Mn, Cu-Ag-Mg, and Fe-Si were combined to form three groups of elements. Similar to A357, cast plates were made with close to the minimum and maximum percentages of each element in each group. The target for those elements not being specifically varied was the middle of the allowed composition range.

Two different solidification rates were achieved by varying the pour temperature and chill material. Copper or iron chills were placed along the center of the plates and pour temperatures of 1350F and 1450F, respectively, were used to obtain two solidification rates. Similar to A357, the Cu- and Fe-chilled
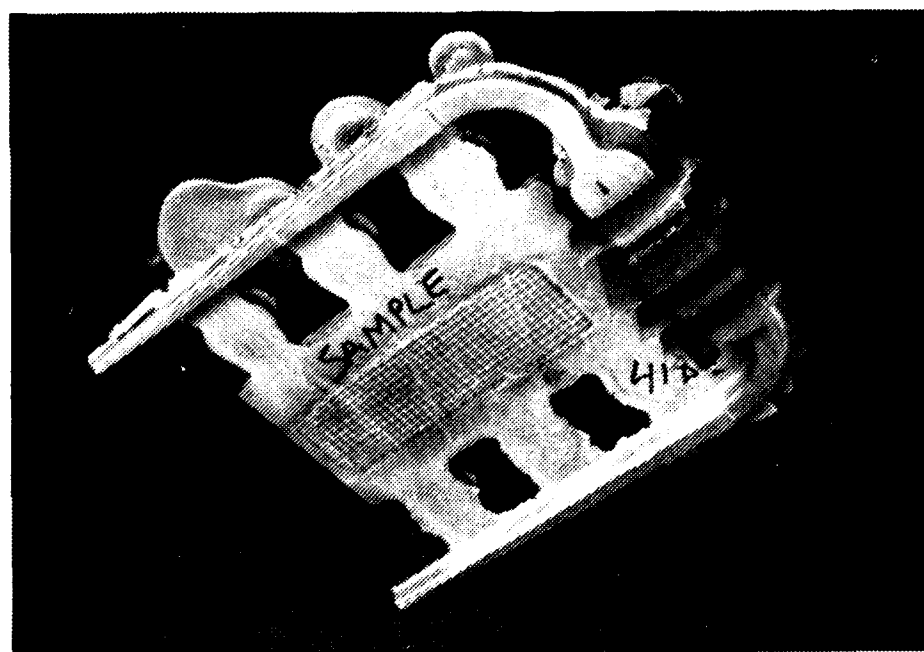
Figure 46. Gating, Risering, and Chill Placement Used
for the A201 Process Variable Plates

Element[1]	Range (wt %)	
	Min.	Max.
Copper	4.5	5.0
Silver	0.5	1.0
Maganese	0.20	0.50
Magnesium	0.25	0.35
Titanium	0.15	0.35
Iron	—	0.05
Silicon	—	0.05
Others, each	—	0.05
Others, total	—	0.15
Aluminum	Balance	

(1) AMS 4242 (Draft 40GD)

Figure 47. Composition Specification for the A201-T7 Screening Plates

COMPOSITION VARIABLES	DEVIATION FROM MID-RANGE CF COMPOSITION SPECIFICATION	
	Min.	Max.
Ti, Mn	X	X
Cu, Ag, Mg	X	X
Fe, Si	(1)	X

(1) Not evaluated

Figure 48. Composition Variations for the A201-T7 Screening Plates

A201 plates are referred to in this report as fast and slow solidification rate plates, respectively.

All plates were hot isostatically pressed (HIPed) to reduce the amount of microshrinkage that can sometimes be present in A201. This step was taken to reduce the number of potential sites for fatigue crack initiation. HIPing was undertaken by step heating the plates up to 950F and holding for 3 hours in an inert gas atmosphere at 15,000 psi.

All 20 plates were solution treated identically. They were held at 940F for 2 hours, 960F for 2 hours, and 980F for 16 hours and then quenched in room temperature water with a maximum quench delay time of eight seconds.

The effect of two different aging temperature/time combinations was evaluated. These were: (a) 360 $\pm$ 5F for 8 hours, and (b) 380 $\pm$ 5F for 5 hours. These combinations were selected following consultations with foundries as being within the range of temperatures and times typically used for aging A201 castings to the T7 condition.

The variations in the three process variables (composition, solidification rate, and aging parameters) provided a total of 20 combinations, as shown in Figure 49.

All plates were Grade B, or better, according to MIL-A-2175. The inspection and composition verification procedures were the same as those for A357, described in Section 5.2.1.

6.2.2 Test Procedures

The A201 screening tests were identical to those described in Section 5.2.2 for A357 except that the net maximum stress for the constant amplitude fatigue life testing was raised to 25 ksi.

6.2.3 Microstructural Characterization

The grain size was measured at both the edge and the center (under the chill) of each plate. The percent porosity in each plate was also determined, using image analysis. The effectiveness of the HIPing in reducing the amount of microshrinkage was confirmed by determining the ultrasonic attenuation in each plate both before and after HIPing.

6.2.4 Data Analysis

Data were analyzed as described in Section 5.2.4 for A357.

6.3 RESULTS AND DISCUSSION

The hardness and conductivity values for each plate were taken after solution heat treatment (SHT) and again after aging. The average hardness of all 20 plates (Rockwell B) was 59 after

| Composition[1] | Slow Solidification | | Fast Solidification | |
| | Aging Parameters | | Aging Parameters | |
	360F/8Hr	380F/5Hr	360F/8Hr	380F/5Hr
Ti, Mn				
Max.	X	X	X	X
Min.	X	X	X	X
Cu, Ag, Mg				
Max.	X	X	X	X
Min.	X	X	X	X
Fe, Si				
Max.	X	X	X	X

(1) Other elements were mid-range of the specification

Note: Each "X" represents one cast plate (total of 20 plates)

Figure 49. Process Variables for the A201-T7 Screening Plates

SHT and 81 after aging. The conductivity (% of IACS) for these materials was 28% and 33%, respectively. The properties are summarized and discussed in the following subsections.

6.3.1 Composition

Melt analyses were supplied by Hitchcock Industries and confirmed by Northrop. Four plates were made for each composition variant (Figure 49). The average contents of the alloying elements that were specifically controlled are summarized in Figure 50. The target for the elements that were not specifically controlled was the mid-range of the specification.

6.3.2 Microstructure

The grain size and percent porosity were determined at two locations in each plate, under the chill and at the edge of the plate. The results are discussed below.

Grain Size

The grain size results are presented in Figure 51. The overall average grain size was 0.0039 inch under the chill and 0.0043 inch at the edge of the plate. Composition had a noticeable effect on these values. The variants with high levels of Ti/Mn or Fe/Si had the smallest average grain sizes. The low Ti/Mn and Cu/Ag/Mg variants had larger-than-average grain sizes. The observed effect of varying the Ti/Mn content is to be expected because Ti is added as a grain refiner. The Ti was added to each melt with the same delay time before pouring. Thus, the observed effect of Ti is not due to variations in the residence time in the melt before pouring.

The solidification rate had the anticipated effect; the faster rate produced a smaller average grain size at the chill (0.0035 inch) than the slower rate (0.0044 inch). The effect of solidification rate was much more pronounced by the low Ti/Mn than by the high Ti/Mn variant, as might be expected. The high levels produced a small grain size even when the solidification rate was slow, indicating that the grain size was relatively independent of solidification rate. The grain size of the high Fe/Si variant was also relatively independent of solidification rate.

Percent Porosity

Similar to the A357 screening plates, an assessment of the percent porosity present in each A201 plate was obtained using the microstructure specimen excised from underneath the chill. Unlike A357, almost no gas or shrinkage porosity was detected in any of the 20 A201 plates. Microshrinkage porosity was sealed by HIPing. Ultrasonic attenuation measurements taken both before and after HIPing confirmed the reduction of microshrinkage. The average ultrasonic attenuation was reduced from 3.21 to 0.59 dB/cm by HIPing.

87

| | Element (Wt %) | | |
Element Content[1]	Ti-Mn	Cu-Ag-Mg	Fe-Si
Max.	0.35-0.43	4.95-0.98-0.32	0.041-0.043
Min.	0.19-0.24	4.65-0.57-0.26	(2)

(1) All other elements were mid-range of the specification
(2) Not evaluated

Figure 50. Composition of the A201 Screening Plates

COMPOSITION[1]	SPECIMEN LOCATION	GRAIN SIZE (10^{-4} IN.)				
		AGE (SLOW SOLIDIFICATION)[2]		AGE (FAST SOLIDIFICATION)[3]		AVG.
		360F/8HR	380F/5HR	360F/8HR	380F/5HR	
0.35Ti-0.43Mn	CHILL	24	33	28	24	27
	EDGE	33	33	28	24	30
0.19Ti-0.24Mn	CHILL	67	79	33	33	53
	EDGE	67	79	47	33	57
4.95Cu-0.98Ag -0.32Mg	CHILL	40	47	40	47	44
	EDGE	56	56	33	47	48
4.65Cu-0.57Ag -0.26Mg	CHILL	47	57	40	47	48
	EDGE	67	67	33	47	54
0.041Fe-0.043Si	CHILL	20	24	33	28	26
	EDGE	28	28	40	28	31
AVERAGE	CHILL	39	48	35	35	39
	EDGE	51	53	36	35	43

(1) Other elements were mid-range of the specification.
(2) Fe chill; 1450F pour temperature.
(3) Cu chill; 1350F pour temperature.

Figure 51. Effect of Process Variables on the Grain Size of A201-T7

89

6.3.3 Tensile Properties

The overall average tensile properties were 65 ksi (UTS), 59 ksi (YS), and 7% elongation, which were significantly higher than the target values (60/50/3). Stress corrosion tests were conducted on A201 from both aging conditions to confirm that the material was in the overaged (T7) condition. Specimens were exposed for 30 days to alternate immersion in salt water at a stress of 37.5 ksi. No failures were experienced. The results for each of the three tensile properties are discussed separately below.

Ultimate Strength

The UTS (Figure 52) was highest for those variants that had the highest levels of Cu/Ag/Mg (69.6 ksi). This is as expected because these are the main strengthening elements added to A201. The lowest UTS (62.3 ksi) was obtained for the plates that contained the maximum levels of Fe and Si impurities. The UTS of the low Ti/Mn variant was slightly greater than that of the high Ti/Mn variant, 65.8 ksi vs. 63.3 ksi.

No effect of solidification rate on the UTS was observed. The UTS was slightly higher (66 ksi) for the plates that were aged at 360F for 8 hours than those aged at 380F for 5 hours (64 ksi).

In summary, the UTS was slightly influenced by composition and aging conditions.

Yield Strength

The yield strength (Figure 53) was dependent upon the leve.s of Cu/Ag/Mg and Ti/Mn. The yield strength was 58 ksi for the :··. Cu/Ag/Mg levels and 64 ksi for the maximum levels. The high Ti/Mn variant had an average yield strength of 58 ksi, while ··· low Ti/Mn variant had an average yield strength of 60 ks1. ··· lowest average yield strength (57 ksi) was obtained for ··· Fe/Si material.

There was no significant effect of solidificat: · ··· yield strength.

A slight difference in yield strength wa: .: · two aging conditions; the 360F/8hr age gave a !.. ·· ksi) than that for material aged at 380F fc: · · This was similar to the trend observed by ··.·

In summary, the yield strength of A. · composition and the aging conditions.

MICROCOPY RESOLUTION TEST CHART

NATIONAL BUREAU OF STANDARDS-1963-A

| COMPOSITION[1] (Wt. %) | AVERAGE ULTIMATE TENSILE STRENGTH (ksi) | | | | |
| | AGE (SLOW SOLIDIFICATION)[2] | | AGE (FAST SOLIDIFICATION)[3] | | AVG. |
	360F/8HR	380F/5HR	360F/8HR	380F/5HR	
0.35Ti-0.43Mn	64.3	61.4	65.0	62.4	63.3
0.19Ti-0.24Mn	66.5	65.6	66.1	65.2	65.8
4.95Cu-0.98Ag-0.32Mg	70.1	69.3	69.8	69.2	69.6
4.65Cu-0.57Ag-0.26Mg	65.2	64.7	65.1	63.8	64.7
0.041Fe-0.043Si	64.5	60.0	64.3	60.3	62.3
AVERAGE	66.1	64.2	66.0	64.2	65.2

(1)Other elements were mid-range of the specification
(2)Fe chill; 1450F pour temperature
(3)Cu chill; 1350F pour temperature

Figure 52. Effect of Process Variables on the Ultimate Tensile Strength of A201-T7

COMPOSITION[1] (Wt. %)	AVERAGE YIELD STRENGTH (ksi)				
	AGE (SLOW SOLIDIFICATION)[2]		AGE (FAST SOLIDIFICATION)[3]		AVG.
	360F/8HR	380F/5HR	360F/8HR	380F/5HR	
0.35Ti-0.43Mn	59.2	56.1	58.5	56.0	57.5
0.19Ti-0.24Mn	61.0	59.8	60.3	59.0	60.0
4.95Cu-0.98Ag-0.32Mg	64.8	63.5	63.8	63.2	63.8
4.65Cu-0.57Ag-0.26Mg	58.5	57.4	58.1	56.4	57.6
0.041Fe-0.043Si	59.0	55.5	58.7	55.5	57.2
AVERAGE	60.5	58.5	60.0	58.0	59.2

(1) Other elements were mid-range of the specification
(2) Fe chill; 1450F pour temperature
(3) Cu chill; 1350F pour temperature

Figure 53. Effect of Process Variables on the Yield Strength of A201-T7

Elongation

The elongation to failure showed (Figure 54) a dependence upon composition. At the higher Cu/Ag/Mg content, the elongation was less than that at the lower Cu/Ag/Mg level, 6.6% vs. 8.8%, respectively. The low Ti/Mn variant had an elongation slightly greater than that of the high Ti/Mn variant, 7.9% vs. 6.3%.

Higher elongation values were obtained at the faster solidification rate (8% vs. 6%).

The elongation to failure was essentially independent of the aging combinations.

In summary, the elongation to failure was mainly influenced by composition and by the solidification rate.

6.3.4 Notched Tensile Strength and NTS/YS Ratio

The notched tensile strength and NTS/YS ratio data are summarized in Figures 55 and 56, respectively. The overall average NTS value was 85.6 ksi. As a function of composition, the NTS ranged from 82.0 ksi (high Fe/Si) to 89.2 ksi (low Ti/Mn). The high Ti/Mn variant had a NTS of 87.2 ksi. Both the high and low Cu/Ag/Mg variants had the same NTS (85.5 ksi).

The average NTS was higher for material solidified at the faster rate (88 ksi vs 84 ksi) than that for the slow solidification rate material.

The 360F/8hr aging condition resulted in a slightly higher NTS than the 380F/6hr age (87ksi vs. 84 ksi).

As a function of composition, the NTS/YS ratio ranged from 1.34 to 1.52, the average value being 1.45. The high and low values were obtained for the high Ti/Mn and high Cu/Ag/Mg variants, respectively.

The ratio was higher (1.50) for the fast solidification rate than that for material solidified more slowly (1.41).

No effect of aging conditions on the NTS/YS ratio was observed.

In summary, the NTS was influenced by composition, solidification rate, and aging condition. The NTS/YS ratio was affected by composition and solidification rate.

6.3.5 Fatigue Life

At least two fatigue specimens from each plate were tested. Where considerable discrepancy between the two results occurred, additional tests were run. The data are summarized in

COMPOSITION[1] (Wt. %)	AGE (SLOW SOLIDIFICATION)[2]		AGE (FAST SOLIDIFICATION)[3]		AVG.
	360F/8HR	380F/5HR	360F/8HR	380F/5HR	
0.35Ti-0.43Mn	7.2	5.2	10.7	2.3	6.3
0.19Ti-0.24Mn	6.2	6.1	9.6	9.5	7.9
4.95Cu-0.98Ag-0.32Mg	4.4	6.0	8.7	7.3	6.6
4.65Cu-0.57Ag-0.26Mg	7.2	8.8	9.5	9.7	8.8
0.041Fe-0.043Si	7.0	5.7	8.6	7.2	7.1
AVERAGE	6.4	6.3	9.5	7.2	7.4

AVERAGE ELONGATION (%)

(1)Other elements were mid-range of the specification
(2)Fe chill; 1450F pour temperature
(3)Cu chill; 1350F pour temperature

Figure 54. Effect of Process Variables on the Elongation of A201-T7

	AVERAGE NOTCHED TENSILE STRENGTH (ksi)				
COMPOSITION[1] (Wt. %)	AGE (SLOW SOLIDIFICATION)[2]		AGE (FAST SOLIDIFICATION)[3]		AVG.
	360F/8HR	380F/5HR	360F/8HR	380F/5HR	
0.35Ti-0.43Mn	85.5	84.2	91.2	87.8	87.2
0.19Ti-0.24Mn	87.3	87.2	91.9	90.5	89.2
4.95Cu-0.98Ag-0.32Mg	81.2	83.9	86.0	91.3	85.6
4.65Cu-0.57Ag-0.26Mg	83.2	80.9	89.0	88.7	85.5
0.041Fe-0.043Si	89.0	74.0	90.0	75.2	82.0
AVERAGE	85.2	82.0	89.7	86.8	85.6

(1)Other elements were mid-range of the specification
(2)Fe chill; 1450F pour temperature
(3)Cu chill; 1350F pour temperature

Figure 55. Effect of Process Variables on the Notched Tensile Strength of A201-T7

COMPOSITION[1] (wt. %)	AGE (SLOW SOLIDIFICATION)[2]		AGE (FAST SOLIDIFICATION)[3]		AVG.
	360F/8HR	380F/5HR	360F/8HR	380F/5HR	
0.35Ti-0.43Mn	1.45	1.50	1.56	1.57	1.52
0.19Ti-0.24Mn	1.43	1.46	1.52	1.53	1.49
4.95Cu-0.98Ag-0.32Mg	1.25	1.32	1.35	1.45	1.34
4.65Cu-0.57Ag-0.26Mg	1.42	1.41	1.53	1.57	1.48
0.041Fe-0.043Si	1.51	1.33	1.53	1.36	1.43
AVERAGE	1.41	1.41	1.50	1.50	1.45

Title above table: AVERAGE NTS/YS RATIO

(1) Other elements were mid-range of the specification
(2) Fe chill; 1450F pour temperature
(3) Cu chill; 1350F pour temperature

Figure 56. Effect of Process Variables on the NTS/YS Ratio of A201-T7

Figure 57. Log average values are quoted. The data scatter was significant, which is not unusual for this type of test. The overall log average fatigue life was 158 x 10^3 cycles. The fatigue life range for the composition variants was 128 x 10^3 to 222 x 10^3 cycles. Considering the amount of data scatter, there were no apparent correlations between fatigue life and any of the three process variables.

6.3.6 Regression Analysis

Linear and nonlinear regression analyses were conducted as described in Section 5.2.4. The results are summarized in Figure 58. The overall approach was the same as that for A357-T6, described in Section 5.3.6.

The Ag content accounted for significant portions of the total percent variation explained in the ultimate and yield strengths and had a smaller effect on the NTS/YS ratio. The data presented in Figures 52 and 53 showed that the combined Cu/Ag/Mg level significantly influenced the tensile strength. Clearly, from the regression analysis, Ag was the main contributor of these three elements.

Ti content showed a strong correlation with grain size and, to a lesser extent, yield strength. Since Ti is added as a grain refiner, the correlation is to be expected and was noted from the data presented in Figure 51.

The percent variations explained in UTS, YS, NTS/YS ratio, and grain size were similar for the linear and nonlinear analyses, indicating that linear relationships probably exist. There was no correlation between fatigue life and the process variables.

The total percent variation explained in the linear analyses for elongation and NTS was reduced to zero in the nonlinear analysis. This reduction probably occurred because the values, 23% and 42%, respectively, were relatively low, and because the error level for the nonlinear analysis was reduced from 5% to 1%. In each case, a weak linear correlation was indicated. For elongation, the linear correlation was with the solidification rate. The NTS correlation was shared equally between Si content and aging condition.

6.4 CONCLUSIONS

The combined conclusions from both the tabulated data and the regression analyses regarding the effect of process variables on the mechanical properties and microstructural features of A201-T7 are as follows.

97

| COMPOSITION[1] | LOG AVERAGE FATIGUE LIFE (10³ CYCLES TO FAILURE)* | | | | |
| | AGE (SLOW SOLIDIFICATION)[2] | | AGE (FAST SOLIDIFICATION)[3] | | AVG. |
	360F/8HR	380F/5HR	360F/8HR	380F/5HR	
0.35Ti-0.43Mn	145	169	135	278	174
0.19Ti-0.24Mn	178	373	190	150	222
4.95Cu-0.98Ag-0.32Mg	157	150	125	131	141
4.65Cu-0.57Ag-0.26Mg	118	137	147	113	128
0.041Fe-0.043Si	147	119	158	122	137
LOG AVERAGE	149	187	149	150	158

*Specimen with a hole; Kt=2.42; net maximum stress=25 ksi.
(1) Other elements were mid-range of the specification.
(2) Fe chill; 1450F pour temperature.
(3) Cu chill; 1350F pour temperature.

Figure 57. Effect of Process Variables on the Fatigue Life of A201-T7

PROPERTY	LINEAR ANALYSIS(1)								NONLINEAR ANALYSIS(2)
	PERCENT VARIATION EXPLAINED BY PROCESS VARIABLES						TOTAL PERCENT VARIATION EXPLAINED		TOTAL PERCENT VARIATION EXPLAINED
	AGING PARAMETERS	SOLIDIFICATION RATE	Ag	Si	Fe	Ti			
UTS	-	-	93	-	-	-	93		98
YS	-	-	73	-	-	23	96		98
EL	-	23	-	-	-	-	23		0
NTS	21	-	-	21	-	-	42		0
NTS/YS	-	25	24	-	20	-	69		58
FATIGUE LIFE	-	-	-	-	-	-	0		0
GRAIN SIZE(3)	-	22	-	-	-	45	67		75

(1) 5% ERROR LEVEL
(2) 1% ERROR LEVEL
(3) AT THE EDGE OF THE PLATE

Figure 58. Linear and Nonlinear Regression Analysis Results for A201-T7

1. **Composition**

   o Higher Cu/Ag/Mg levels increased UTS and YS, and reduced
     EL and the NTS/YS ratio.
   o The high Fe/Si levels provided the lowest UTS, YS, and
     NTS values.
   o High Ti/Mn levels slightly decreased the UTS, YS, and EL,
     but gave the highest NTS/YS ratio.

2. **Solidification Rate**

   o The faster solidification rate increased ductility, NTS,
     and the NTS/YS ratio.

3. **Aging Temperature/Time**

   o The 360F/8hr aging condition gave higher average UTS,
     YS, and NTS values than those for material aged at 380F
     for 5 hours.

4. **Property Optimization**

   The requirements for optimizing the DADT and tensile
   properties of A201-T7 do not conflict.

6.5 RECOMMENDATIONS

1. The approved AMS 4242 specification should be used for
   producing the A201-T7 verification plates for the remaining
   portion of Task 2, Phase I, and for the plates required for
   Task 3, Phase I.

2. The plates for subsequent DADT characterization on the
   DADTAC program should have a maximum grain size of 0.0035".
   This may be obtained through Ti additions and/or chilling,
   which will also minimize the formation of shrinkage sponge.

REFERENCES

1. L. Adler, J. Rose, and C. Mobley, _J. Appl. Phys._ 59, p. 336, 1986.

2. J. Gubernatis and E. Domany, _Review of Progress in Quantitative Nondestructive Evaluation_, edited by D. Thompson and D. Chementi, Plenum, New York, 1983, Vol 2A, p 833.

3. P. Nagy, D. Rypien, and L. Adler, To be published.

4. Aerospace Material Specification, AMS 4241, 1986, Society of Automotive Engineers, Warrendale, PA 15096.

5. Northrop Process Specification IT-72.

6. Chamberlin, B. and Sulzer, J., "Gas Content and Solidification Rate Effect on Tensile Properties and Soundness of Aluminum Casting Alloys," _Modern Casting_, Vol. 46, Oct., 1964.

7. James, M.R. and Morris, W.L., "The Fracture of Constituent Particles During Fatigue," _Material Science and Engineering_, Vol 56, 1982, pp. 63-71.

8. Saunders, D.S., Parker, B.A., and Griffiths, J.F., "The Fracture Toughness of an Aluminum Casting Alloy," _Journal of Australian Institute of Metals_, 1975.

9. Hanna, M.D., Lu, S.Z., and Hallawell, A., "Modification in the Aluminum Silicon System," _Metallurgical Transactions_, Vol. 15A, March, 1984.

10. Turk, G.R., "Fatigue Performance and Phase Structure of 3XX Cast Aluminum Alloys due to Cerium Additions and Anodic Coatings," MS Thesis, University of VA, May 1985.

11. Aerospace Material Specification, AMS 4242, 1986, Society of Automotive Engineers, Warrendale, PA 15096.

END
DATE
FILMED

JAN
1988